Chapter- 4

Synthesis of Fe_3O_4 Nanoparticles Using Different Amino Acid Molecules as Templates, Their Characterization and Applications as Vehicle for Drug Delivery

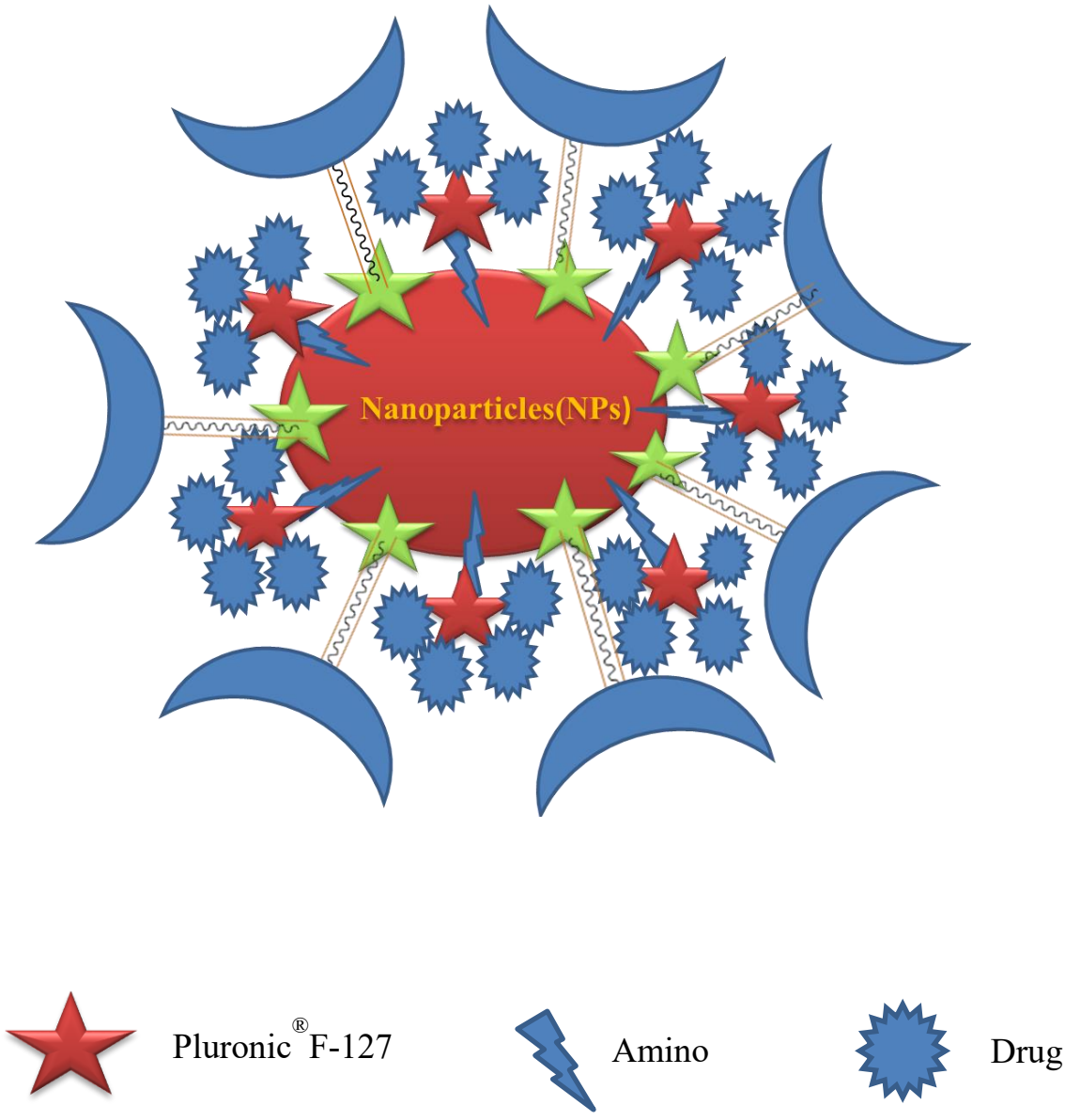

4.1 Introduction

Nowadays, nanoscience and nanotechnology are a advantageous to the patients suffering from diseases like cancer. It requires early and explicit diagnosis followed by target specific treatment [1,2]. Conventional treatments like chemotherapy are vigorous and non-specific. Preferably, factors like effectiveness of the drugs for the disease, immune response, ability of the patient toward drug dosage etc. should be considered before adopting these treatments. Even though they are quite successful, traditional medications (such as taxol, cis-platin, paclitaxol, etc.) have a lot of adverse effects because they are nonspecific and insoluble in bodily fluids [3,4]. For this reason, numerous strategies have been devised. For instance, a medication may become trapped in micelle or nanocavity carriers with hydrophilic or hydrophobic surfaces, such as cyclodextrin. Nevertheless, this has the drawback of the vehicle being broken down by enzymes as it enters the target cells. Furthermore, cell transfection is still a significant problem even if the drug-loaded vehicle manages to reach the target cells (Figure 4.1 and 4.2) [5-10].

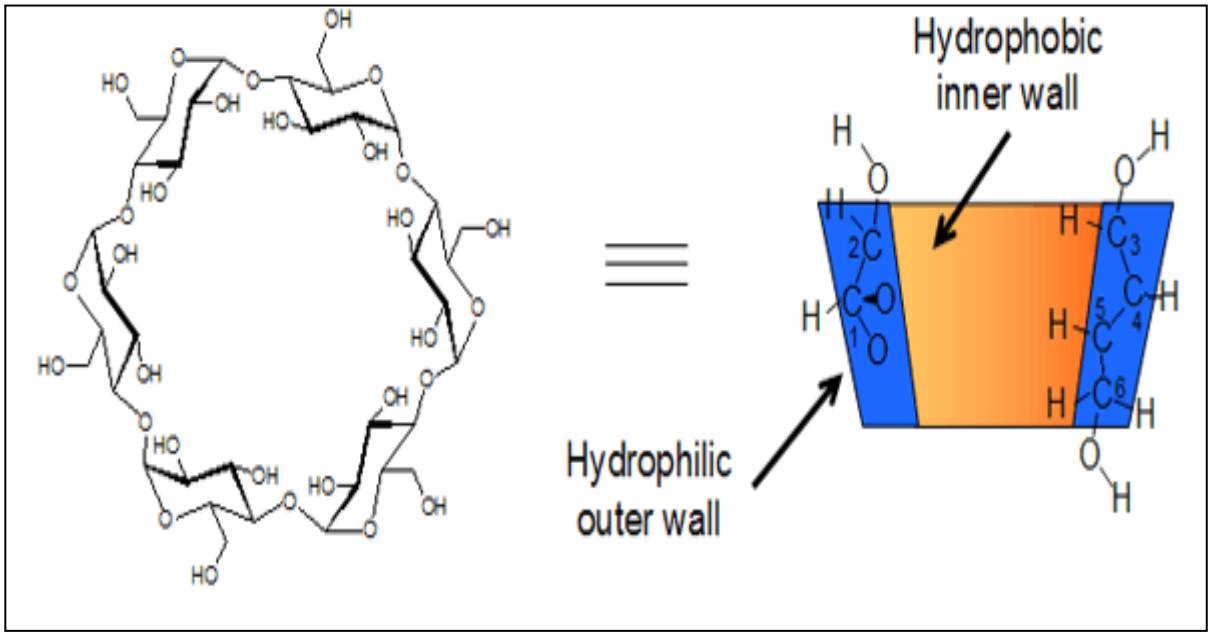

Fig. 4.1. Structure of Cyclodextrin

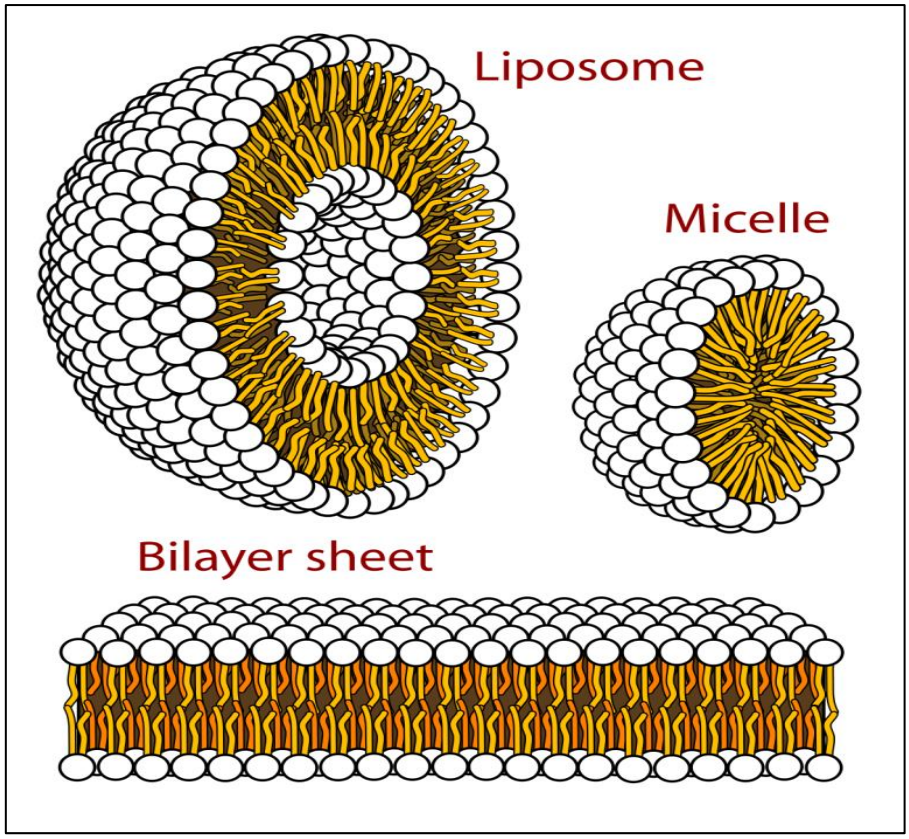

Fig. 4.2. Lipid bilayers.

SPIONs, surface-engineered superparamagnetic iron oxide nanoparticles, are the most effective alternative for this purpose.

(1) The particle size, shape, and surface charge can be adjusted to meet specific requirements. Particles larger than 200 nm are eliminated from the body by the liver, spleen, and reticuloendothelial system (RES), whereas those smaller than 5 nm are quickly expelled by the kidney. Varying the hydrophilic/hydrophobic nature of coating materials surrounding a particle's core can lengthen its circulation lifetime in the blood.

The hydrophilic-lipophilic balance (HLB) within the carrier carrying the drug is very important to decide the stability of drug-vector conjugate in the intracellular environment. Generally, outer surface of the vector is PEGlated to increase the blood circulation and accumulation time. However, it reduces the cellular uptake due to hindrance between cell membrane and carrier known as 'PEG dilemma' [11 -13]. Hence, it is desired that the outer PEG layer of the developed nanocarrier should be detached before cellular entry. Pluronic® F-127 can become alternative for this. Pluronic® F127 (EO102PO78EO102) is an amphilic triblock copolymer. Above CMC, its hydrophobic propylene oxide (PO) blocks self-assemble

into the inner core while, hydrophilic ethylene oxide (EO) blocks form outer corona that result in the formation of stable polymeic micelle in the intracellular environment [14,15]. It has been observed that the incorporation of drugs into the hydrophobic PO core of these micelles increases the solubility, metabolic stability and circulation time during its journey towards the target [15]. However, very less studies are available showing the use of pluronic for drug delivery [16]. The advantages of using pluronic for the formation of stealth outer surface as an alternative to PEG are: (1) being amphiphilic in nature, it is conducive to both drug/gene and intracellular environment prolonging the circulation time, (2) it has been observed that strong positively charged carriers are removed rapidly by the reticuloendothelial system (RES) [17]. In case of pluronic, a weakly cationic character results due to oxonium ion formation with water protons or the sharing of the hydrogen in water by H-bonding [18]. Thus, the attractive interaction between this weak polycation and the negative cell surface synergistically enhances transformation and accumulation time.

Brigatinib (Alunbrig®) is an oral, potent and selective anaplastic lymphoma kinase (ALK) and c-ros oncogene 1 (ROS1) tyrosine kinase inhibitor approved for treating adults with advanced ALK-positive non-small-cell lung cancer (NSCLC) not previously treated with an ALK inhibitor. It also exhibits selectivity against 9 different crizotinib-resistant mutants of the EML4-ALK fusion gene, responsible for the transformation of susceptible lung parenchyma. Brigatinib therapy extends the first-line treatment options available for patient including patients with CNS metastases[19,20].

Brigatinib represents the most clinically advanced phosphine oxide-containing drug candidate to date and is currently being evaluated in a global phase 2 registration trial. The fact that tyrosine kinase inhibitor (TKI) associated (inhibits) protein, which is responsible for activating a cascade of proteins that govern the cell cycle and accelerate cell division, demonstrates its utility in the treatment of the disease [21].

Brigatinib (ALK, a signal transduction inhibitor) is one of the TKIs [22]. However, The most common adverse reactions (≥25%) with brigatinib are diarrhea, fatigue, nausea, rash, cough, myalgia, headache, hypertension, vomiting, and dyspnea [23-25]. These shortcomings must be addressed in order to better control the treatment. The majority of these undesirable and harmful effects result from the drug's dispersion throughout the body. If brigatinib is targeted directly to the cancer cells (lung cancer, in this case) the maximum response with minimum side effects can be achieved.

SPIONs can perform this job very well because of the strategy of extending their time at the target site through controlled release of a predetermined amount of the drug while monitoring

disease abatement progress. The idea behind using Fe_3O_4 as a vehicle to load brigatinib and target bone marrow is as follows.

The production of hemoglobin occurs in the developing red blood cells in the bone marrow, a process known as erythropoiesis. Because iron is the primary component of hemoglobin, a large amount of iron is used throughout this process. Oral iron has the advantage of being simple and inexpensive, but it is constrained by adverse effects, low compliance, poor absorption, and low efficacy. The most effective method of iron administration to the bone marrow is intravenous [26]. Iron forms a compound with the transferrin protein found in plasma. The transferrin receptors on the surface of the bone marrow cell line quickly recognized this iron-protein combination and allowed it to enter the cell. When the drug is delivered to the bone marrow, iron oxide NPs naturally accumulate as a precursor of hemoglobin for erythropoiesis.

In the present work, we have reported the synthesis of iron oxide nanoparticles using three amino acids (AA-L-Tyrosine, L-Proline and L-Histidine) as a capping agent. Pluronic- F127, a surfactant triblock co-polymer, was used to encapsulate the AA/Fe_3O_4 NPs. The resulting magnetic micelles, with AA capped Fe_3O_4 NPs as the core and the pluronic surfactant as the shell, were transfected into a human bone marrow MCF7 and A549 cell-lines *in vitro* to evaluate cell death.

4.2. Experimental

4.2.1. Materials

Ferric Chloride ($FeCl_3.6H_2O$) was obtained from Loba chemicals, India. Ferrous Chloride ($FeCl_2.2H_2O$), L-Tyrosine, L-Proline, L-Histidine and, sodium hydroxide (NaOH) were purchased from S D Fine Chemicals, India. Pluronic F-127 was purchased from Sigma Aldrich. All chemicals were AR grade and used without further purification. Chloroform, phenol, isopropanol was purchased from Merck.

4.2.2. Synthesis of Fe_3O_4/AA NPs

Fe_3O_4 NPs were synthesized by simple co-preipitation method. Aqueous ammonia solution (400µL) was dropwise added to the mixture of 50 mL aqueous solution of $FeCl_3.6H_2O$ (0.24 mmol) and $FeCl_2.2H_2O$ (0.121 mmol). To this solution, 25 mL of aqueous solution of amino acid (0.24 mmol) was added and the temperature of reaction mixture was gradually raised to 70 ^oC. The reaction mixture was further stirred thoroughly for about 1 h to obtain a

homogenous mixture. The reaction mixture was further stirred for 24 h to obtain stable homogenized dispersion. The reaction mixture was then centrifuged at 8000 rpm for 5 min and subsequently washed several times with water and ethanol to remove unreacted impurities and dried at 70 ^{o}C under vacuum for two days (Figure 4.3).

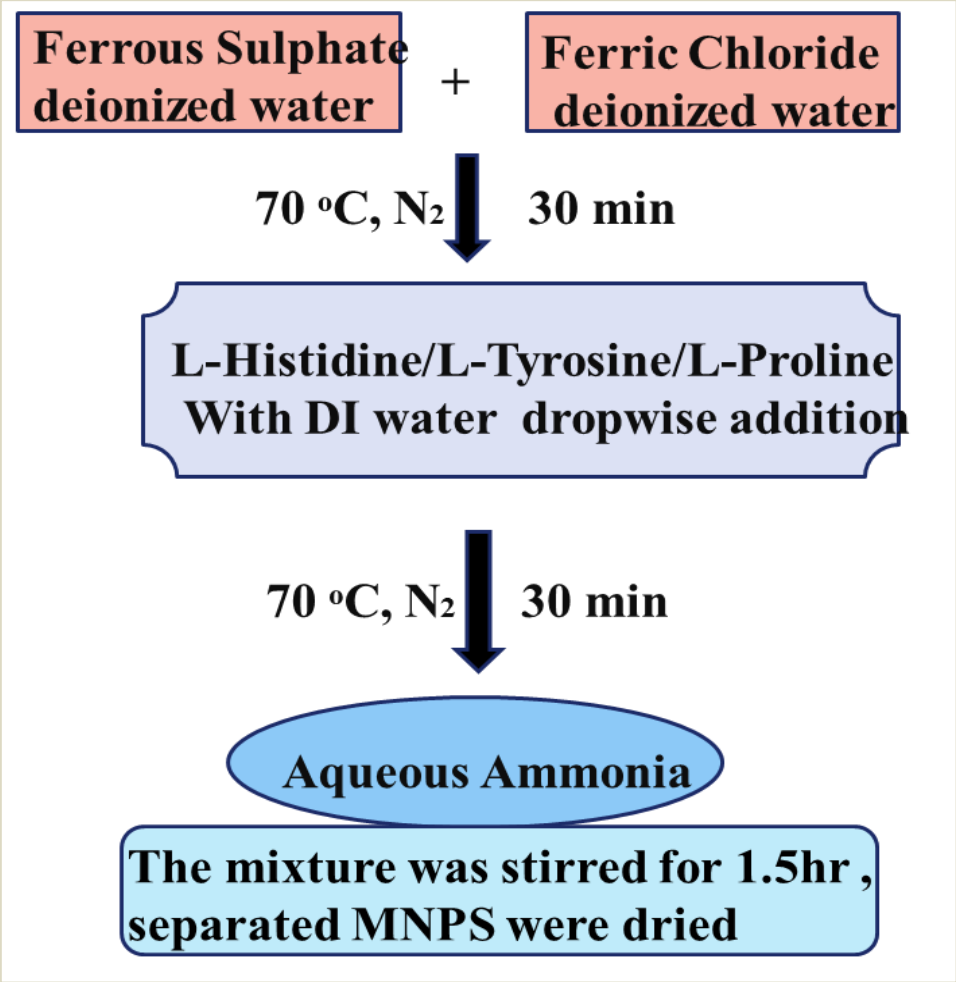

Fig. 4.3. Synthesis of imatinib loaded Fe_3O_4/EDTA/P magnetic micelles.

300 mg of Fe_3O_4/AA nanoparticles were dispersed in 30 mL of milliQ water and then 100 mg of pluronic F-127 was added. The mixture was then stirred overnight on a magnetic stirrer at RT and then centrifuged at 6000 rpm for 5 min to get pluronic- F127 functionalized Fe_3O_4/AA NPs. 30 mg of these nanoparticles were dispersed in 10 mL of milliQ water. To it, 2 mL of a suspension containing the drug solution (4.5 mg/mL) was added. Then the mixture was stirred vigorously on the magnetic stirrer at RT for about 24 h. The drug-loaded Fe_3O_4 nanoparticles were allowed to settle down by a magnet. The magnet was kept outside the flask containing drug-loaded nanoparticles for about 6 h and then the supernatant was

decanted. The drug-loaded nanoparticles were suspended in milliQ water and washed twice (Scheme 4.1).

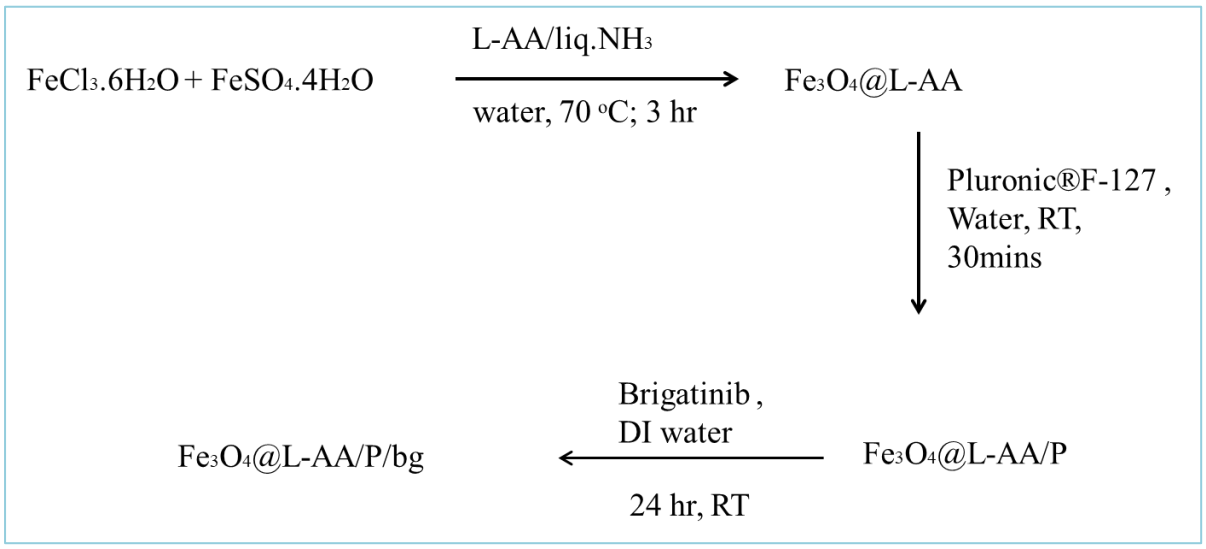

Scheme 4.1. Synthesis of brigatinib loaded Fe_3O_4@ L AA/P magnetic micelles (Fe_3O_4@L AA/P/bg).

The amount of drug-loaded on nanoparticles was calculated by using UV-visible spectroscopy. For that, a drug solution varying in concentration from 0.5 to 9.0 mg/mL was prepared to construct a calibration curve. It was found that for every 1 mg of NPs, 0.121 mg (121.65 mg) of drug was loaded out of 0.150 mg bare drug.

Loading efficiency (%) =

(Weight of drug-loaded/weight of total drug added) x 100……. (1)

Drug loading percentage =

The mass of loaded drug/the mass of initial drug and carrier x 100….(2)

The drug loading efficiency and drug loading percentage were found to be 40.56 and 10.52% respectively.

4.3. Characterization of synthesized Fe_3O_4/AA NPs.

X-ray powder diffraction (XRD) pattern of the Fe_3O_4/AA NPs were obtained from X-ray powder diffractometer (Bruker D8 Advance) with Cu Kα radiation, λ = 0.15418 nm. The mode of interaction of AA with the surface Fe ions of Fe_3O_4 NPs and the structure of magnetic micelles were assessed by Fourier transform infrared spectroscopy (RX-FTIR, Perkin- Elmer, USA). The morphology of the samples was examined by transmission electron microscopy (TEM, Philips Tecnai 20) at 200 kV. All measurements were made at 25

^{o}C in deionized water. Differential Scanning Calorimetric (DSC) analysis and ThermoGravimetric Analysis (TGA) of Fe_3O_4/AA and Fe_3O_4/AA/P samples were carried out using Mettler Toledo DSC 822. For the purpose, the material was heated inside a DSC setup. The heating rate was 10 ^{o}C min^{-1} from RT to 500 ^{o}C in N_2 atmosphere. The magnetic properties were studied on a vibrating sample magnetometer (VSM, Lakeshore 7410) at 298 K under an applied magnetic field of 15.000E+3 G.

4.4. Results and Discussion

The synthesized iron oxide nanoparticles were characterized by XRD to study crystallinity and phase of the material (Figure 4.4). The XRD patterns manifest predominant diffraction peaks at 2θ values 30.1, 35.15, 43.10, 53.50, 57.21 and 63.0 correspond to the (200), (311), (400), (422), (511), and (440) planes, respectively. These features indicate the magnetite phase with inverse spinel structure in which oxygen forming cubic face centered packed (FCC) arrangement and Fe cations occupy the interstial Td and Oh sites. These standard peak positions indicate that coating of edta on Fe_3O_4 NPs as capping ligands does not affect the phase and crystallinity of the material. The particle size calculated from Debye-Scherrer formula ($L=0.9\lambda / \beta \cos\theta$) and the FWHM (Full Width at Half Maximum) values corresponds to the major plane (311) was in the range of 50 nm. The compactness and clear resolution of the peaks indicate properly ordered and compact AA layer on the surface of NPs.

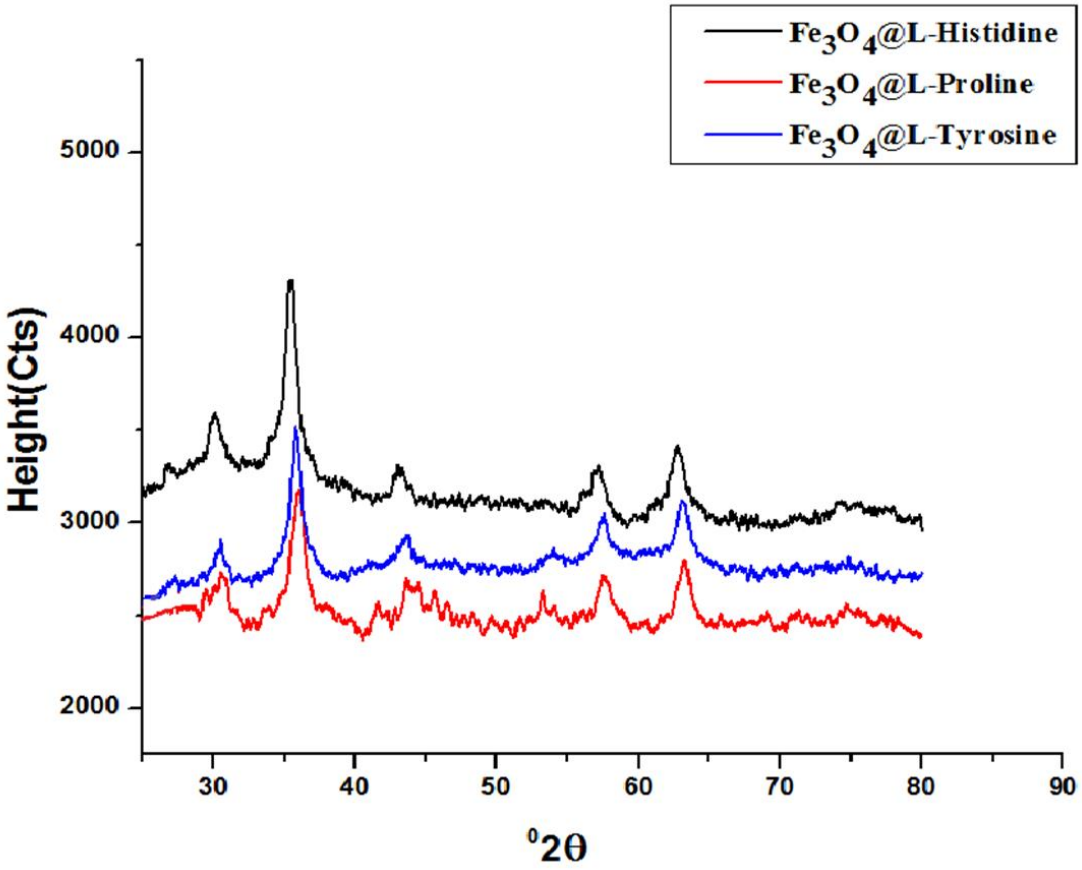

Fig. 4.4. XRD patterns of as-synthesized Fe_3O_4/AA nanoparticles.

The morphologies of as-synthesized Fe_3O_4 NPs were also studied by FESEM analysis (Figure 4.5). FESEM images display an almost uniform size distribution.

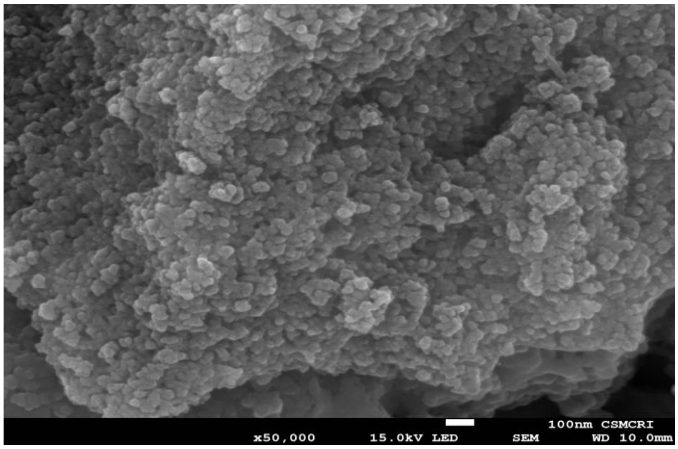

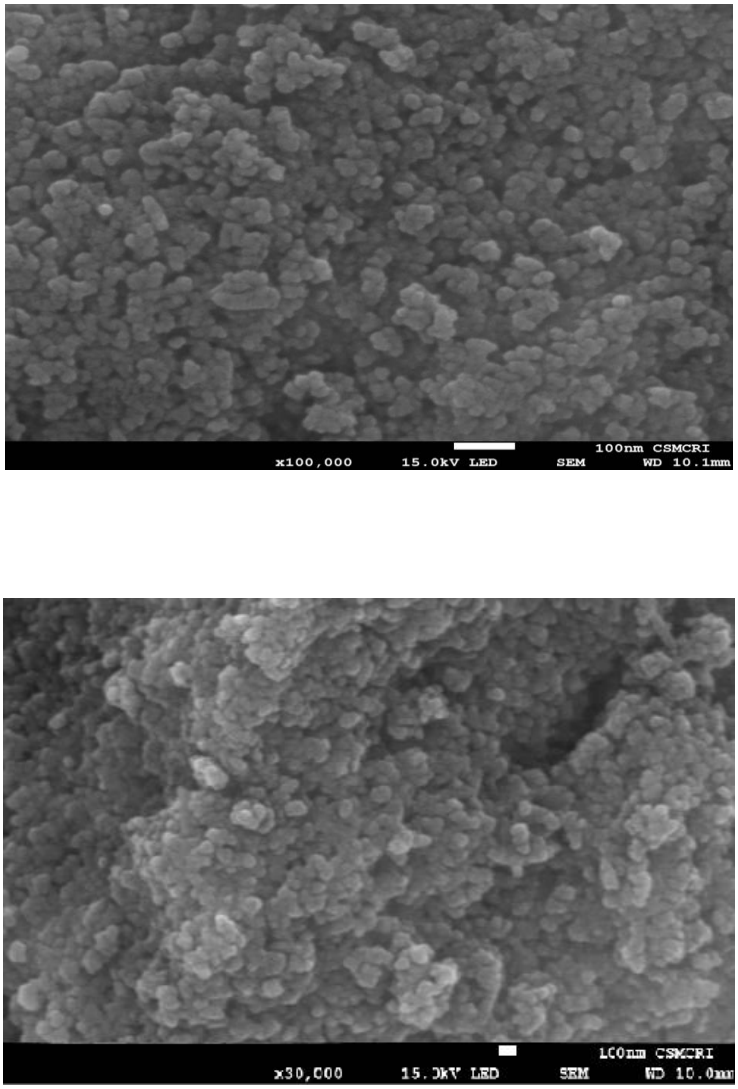

Fig. 4.5. HRSEM images of (a) Fe_3O_4@L-Tyr (b) Fe_3O_4@L-Hist NPs (c) Fe_3O_4@L-Pro NPs.

Further, the size and shape of Fe_3O_4/AA NPs were studied by TEM analysis. The TEM image shows almost monodispersed spherical particles with an average size 5-10 nm (Figure 4.6). The small value of polydispersity index for Fe_3O_4/AA/P system suggests ordered orientation of NPs assembly in aqueous media. In this study, AA plays dual role, first it acts as a capping agent and restrict the growth of Fe_3O_4 crystal to the nano regime. Secondly, AA can increase the adaptation of Fe_3O_4 NPs by the cellular system, compatibilize it completely and, by this way it can reduce the toxicity of the material.

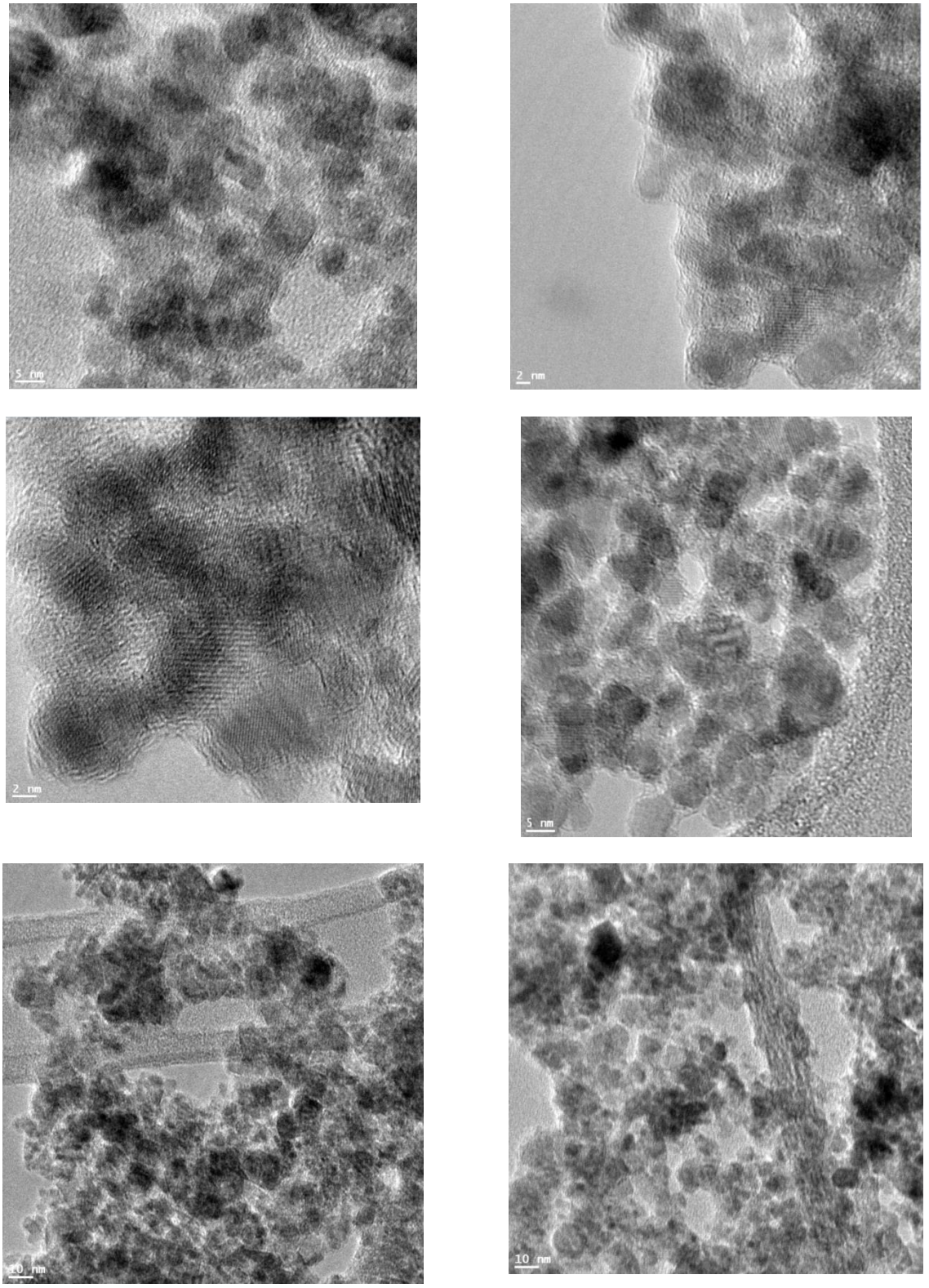

Fig. 4.6. HRTEM images and lattice fringes at higher magnification of as-synthesized (A, D) Fe_3O_4@L-tyr and (B, E) Fe_3O_4@L-pro and (C, F) Fe_3O_4@L-Hist NPs.

To understand the interactions of the AA ligands with the surface of Fe_3O_4 NPs, vibrational spectroscopy (FTIR) is one of the best tools. Figure 4.7 show the FTIR spectrum of Fe_3O_4/AA and Fe_3O_4/AA/P assembly respectively. The absorption at 646 cm^{-1} is corresponds to Fe-O stretching in Fe_3O_4 inverse spinel system. Absorptions in the range of 1110-1180 cm^{-1} are due to presence of block copolymer completely encapsulating the NPs surface and $–CH_2-$ rocking of pluronic respectively. AA possesses one nitrogen atom and one carboxylate anions (in basic media) to coordinate with surface iron (II/III) ions. The carboxylate ions can coordinate with surface iron ions either in a unidentate or a bidentate (chelating) ways. This can be confirmed on the basis of COO^- stretching vibration frequencies. Carboxylate ions in free acetate form vibrate in two fundamental modes, asymmetric stretching *vas* (COO^-) and symmetric stretching *vs* (COO^-) at 1583 and 1422 cm^{-1} respectively. If carboxylate ligand coordinate with surface Fe (II/III) as a bidentate mode then νas (COO^-) decreases and νs (COO^-) increases from the above normal modes in free state and vice versa in case of monodentate mode. On comparing Δ (νas COO^-) - *vs* (COO^-)) with Δ'(*v'as* (COO^-)– *v's* (COO^-)), (where Δ is a difference in the absorption bands for free carobylate ions and Δ' is for metal bound carboxylate ions), we found Δ>Δ'. This suggests bidentate coordination (Figure 4.7).

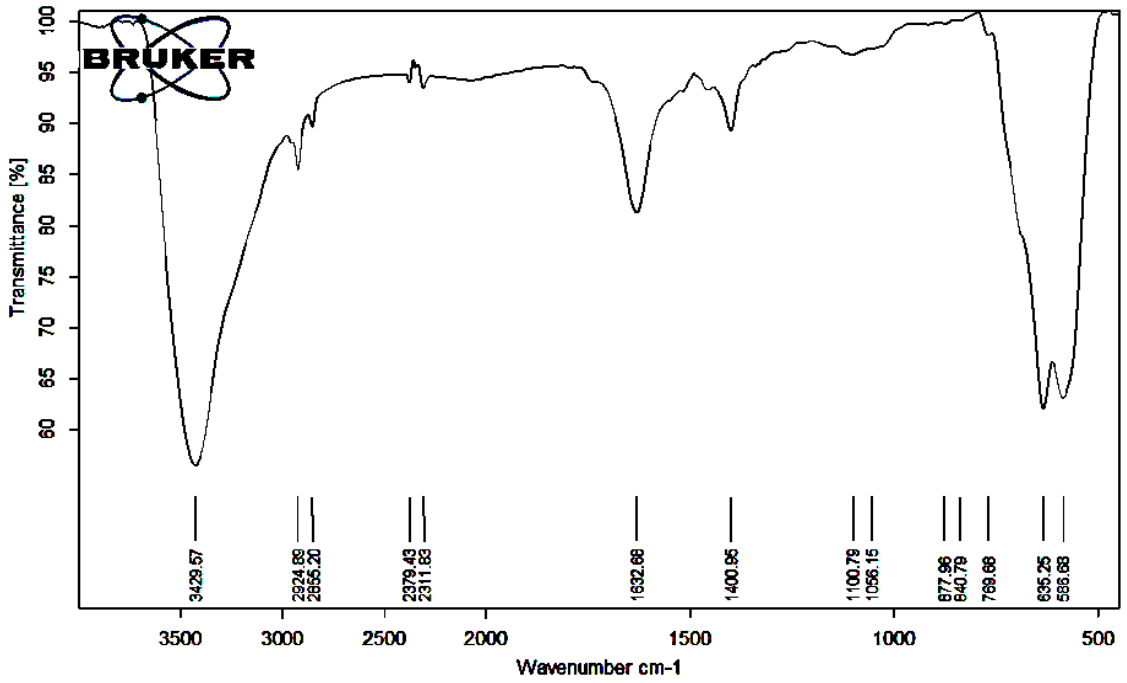

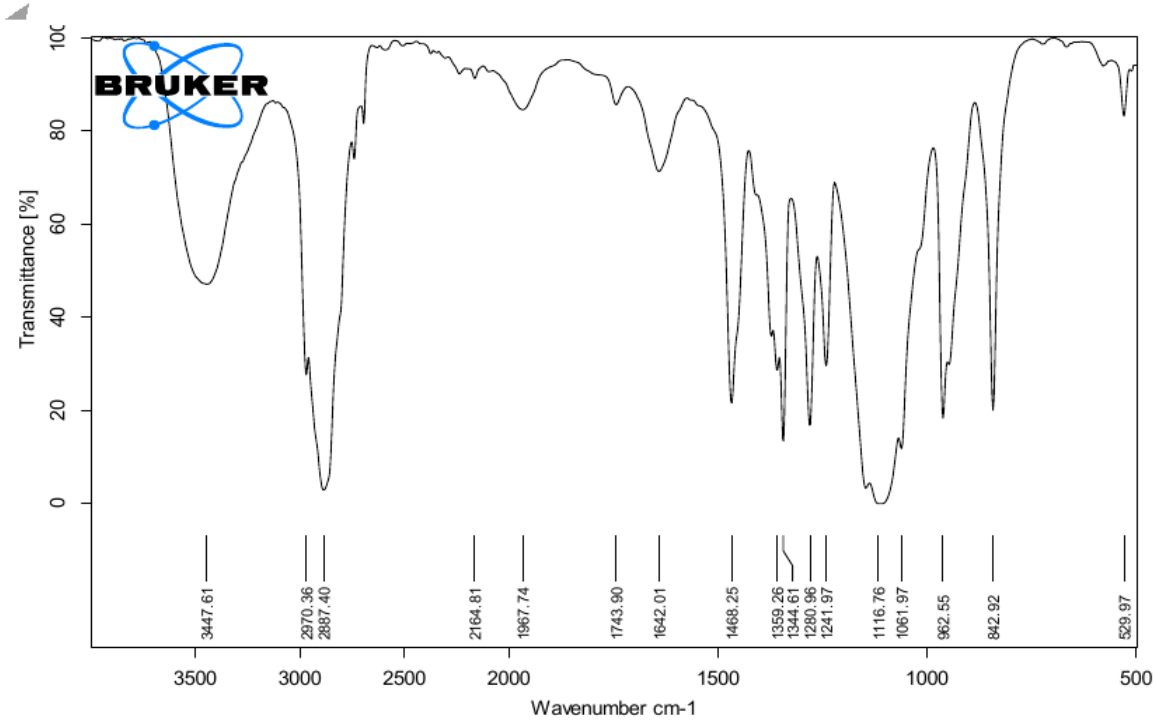
BRUKER
Transmittance [%]
0
20
40
60
80
100
3447.61
2970.36
2887.40
2164.81
1967.74
1743.90
1642.01
1468.25
1359.26
1344.61
1280.96
1241.97
1116.76
1061.97
962.55
842.92
529.97
3500
3000
2500
2000
1500
1000
500
Wavenumber cm-1

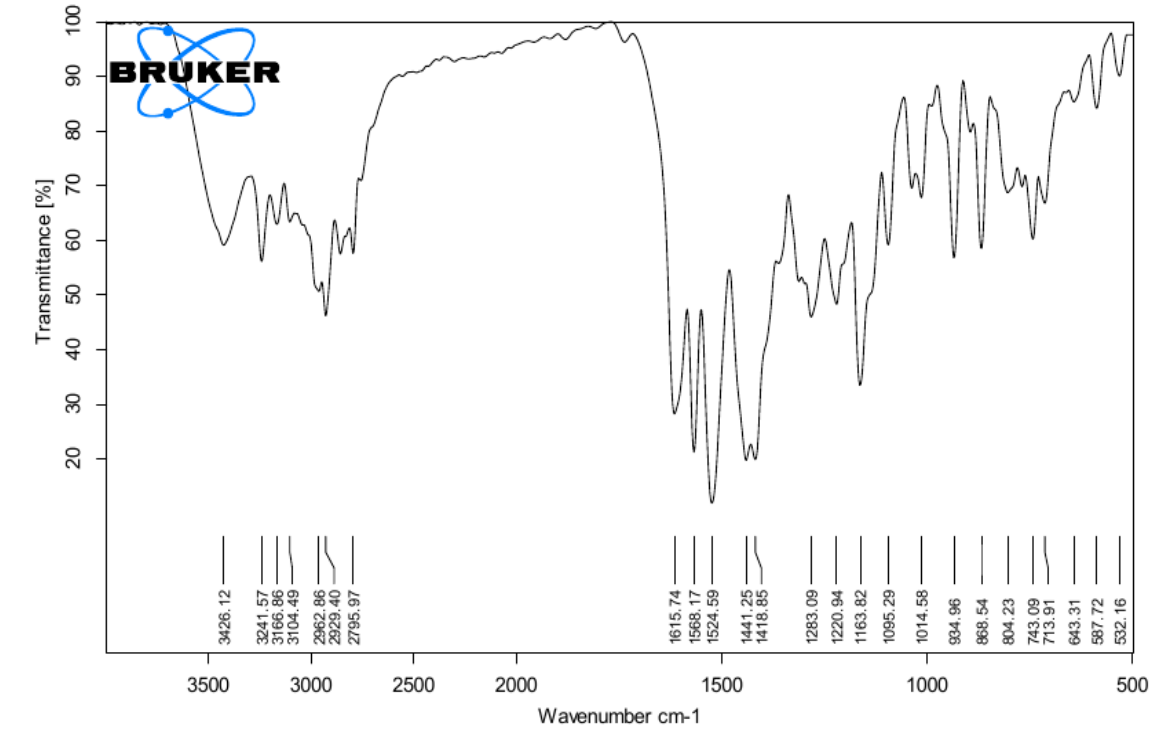
BRUKER
Transmittance [%]
20
30
40
50
60
70
80
90
100
3426.12
3241.57
3166.86
3104.49
2962.86
2929.40
2795.97
1615.74
1568.17
1524.59
1441.25
1418.85
1283.09
1220.94
1163.82
1095.29
1014.58
934.96
868.54
804.23
743.09
713.91
643.31
587.72
532.16
3500
3000
2500
2000
1500
1000
500
Wavenumber cm-1

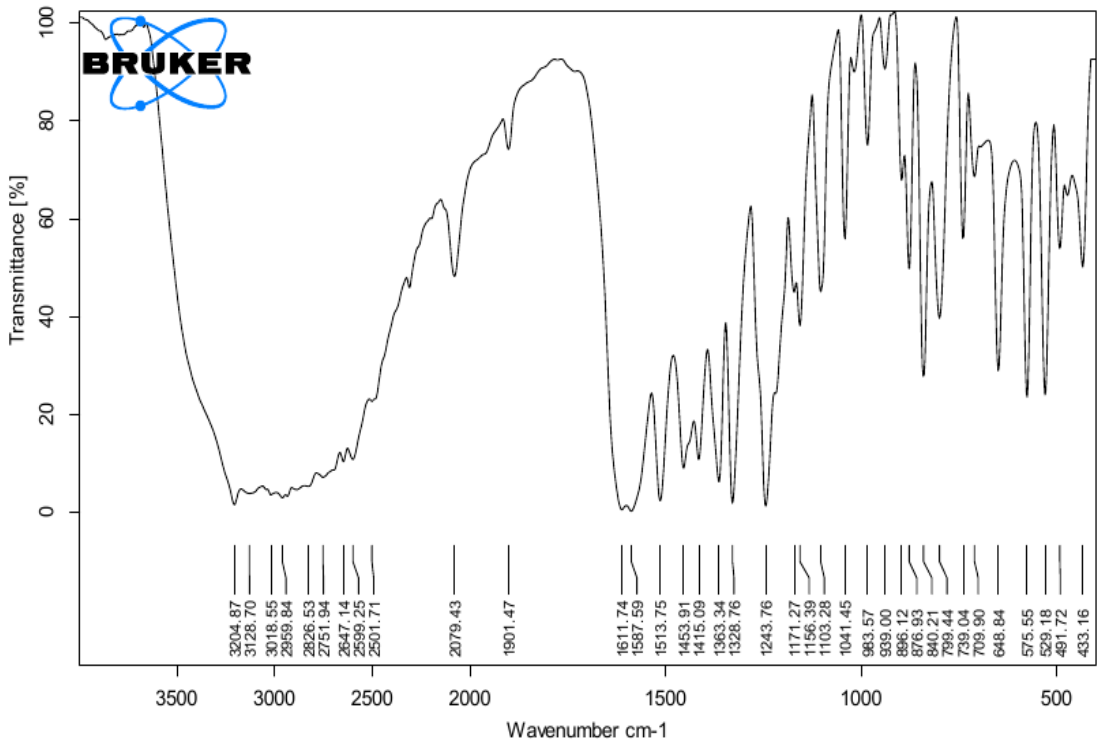
BRUKER
Transmittance [%]
0
20
40
60
80
100
3204.87
3128.70
3018.55
2959.84
2826.53
2751.94
2647.14
2599.25
2501.71
2079.43
1901.47
1611.74
1587.59
1513.75
1453.91
1415.09
1363.34
1328.76
1243.76
1171.27
1156.39
1103.28
1041.45
983.57
939.00
896.12
876.93
840.21
799.44
739.04
709.90
648.84
575.55
529.18
491.72
433.16
3500
3000
2500
2000
1500
1000
500
Wavenumber cm-1

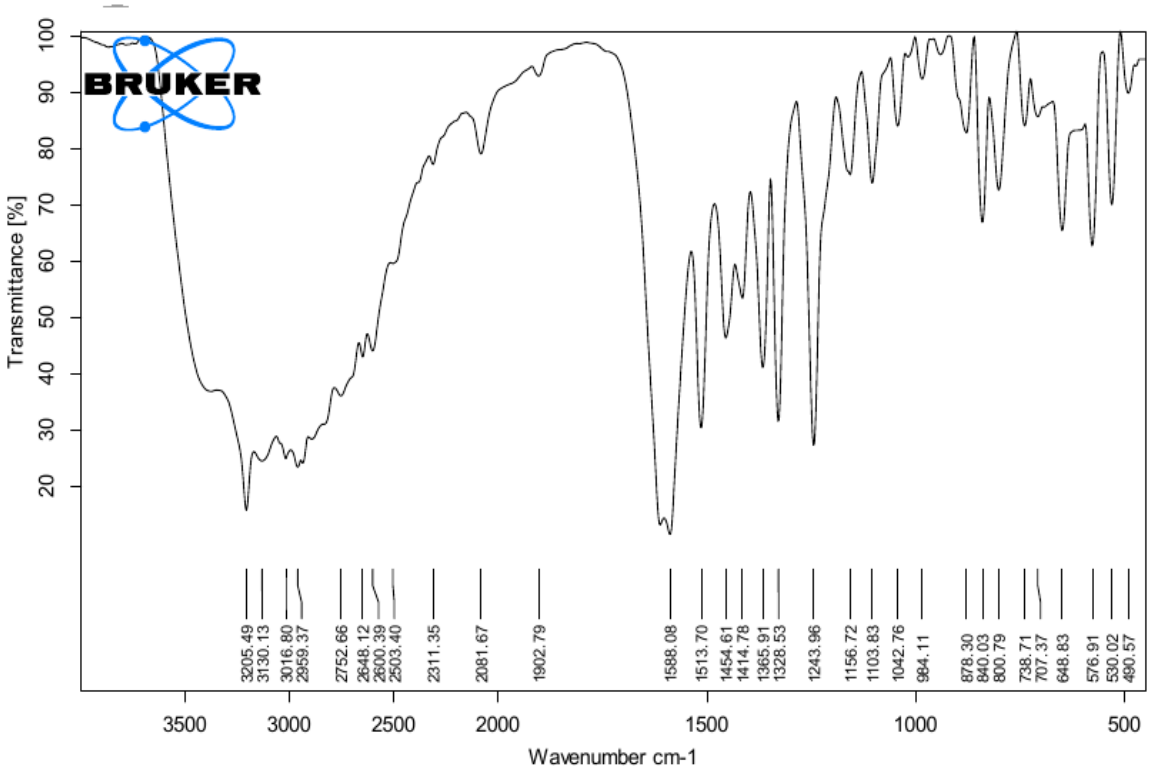
BRUKER
Transmittance [%]
20
30
40
50
60
70
80
90
100
3205.49
3130.13
3016.80
2959.37
2752.66
2648.12
2600.39
2503.40
2311.35
2081.67
1902.79
1588.08
1513.70
1454.61
1414.78
1365.91
1328.53
1243.96
1156.72
1103.83
1042.76
984.11
878.30
840.03
800.79
738.71
707.37
648.83
576.91
530.02
490.57
3500
3000
2500
2000
1500
1000
500
Wavenumber cm-1

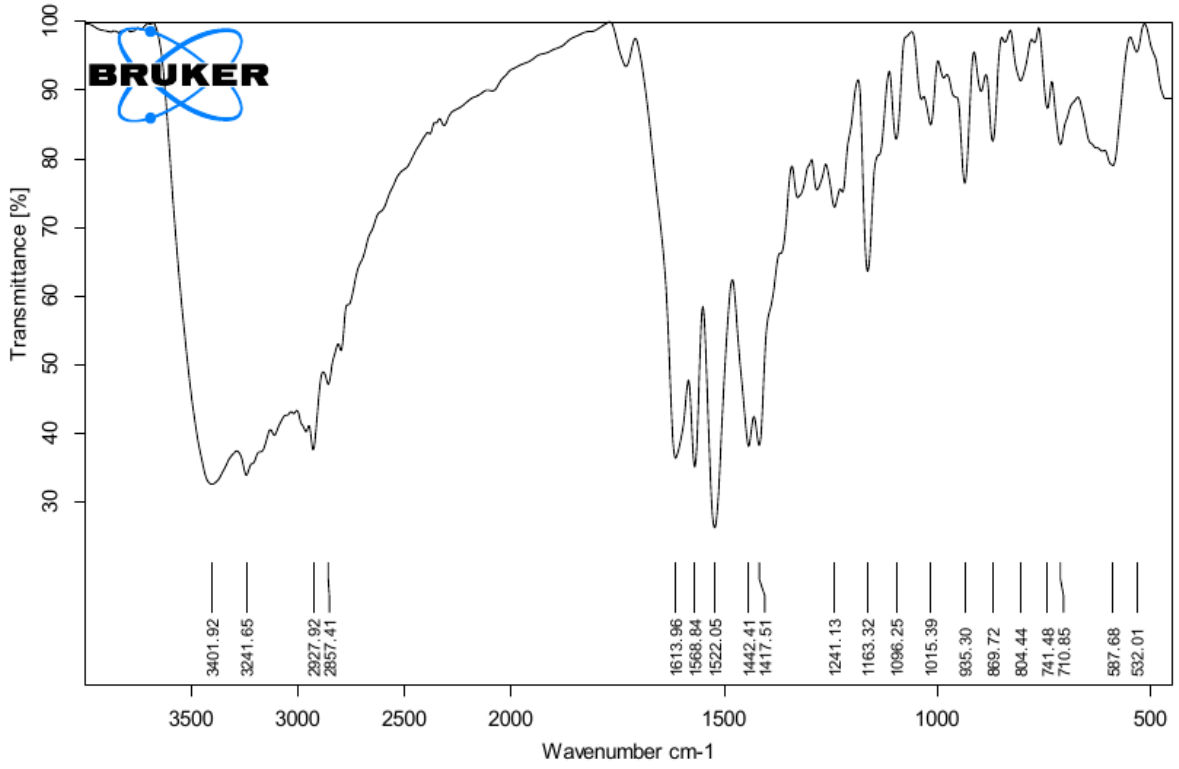
BRUKER
Transmittance [%]
100
90
80
70
60
50
40
30
3401.92
3241.65
2927.92
2857.41
1613.96
1568.84
1522.05
1442.41
1417.51
1241.13
1163.32
1096.25
1015.39
935.30
869.72
804.44
741.48
710.85
587.68
532.01
3500
3000
2500
2000
1500
1000
500
Wavenumber cm-1

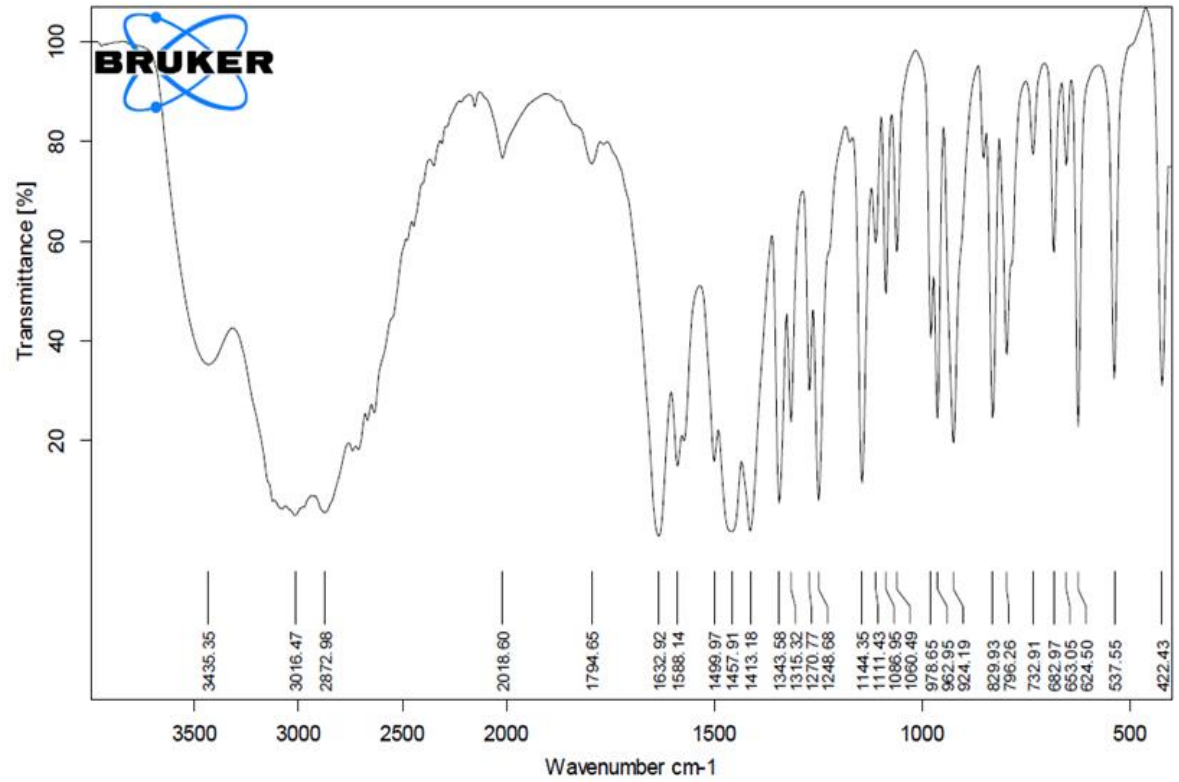
BRUKER
Transmittance [%]
100
80
60
40
20
3435.35
3016.47
2872.98
2018.60
1794.65
1632.92
1588.14
1499.97
1457.91
1413.18
1343.58
1315.32
1270.77
1248.68
1144.35
1111.43
1086.95
1060.49
978.65
962.95
924.19
829.93
796.26
732.91
682.97
653.05
624.50
537.55
422.43
3500
3000
2500
2000
1500
1000
500
Wavenumber cm-1

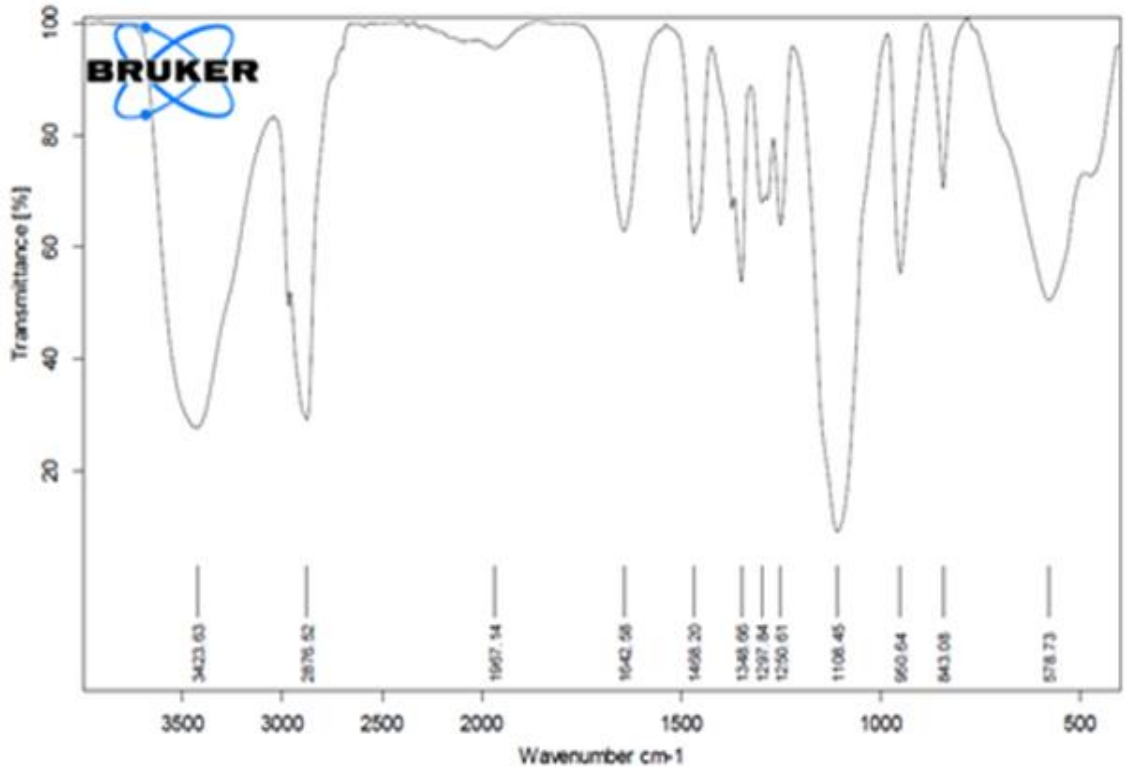
BRUKER
Transmittance [%]
100
80
60
40
20
3423.63
2876.52
1997.14
1642.58
1458.20
1348.66
1297.84
1250.61
1108.45
950.64
843.08
578.73
3500
3000
2500
2000
1500
1000
500
Wavenumber cm-1

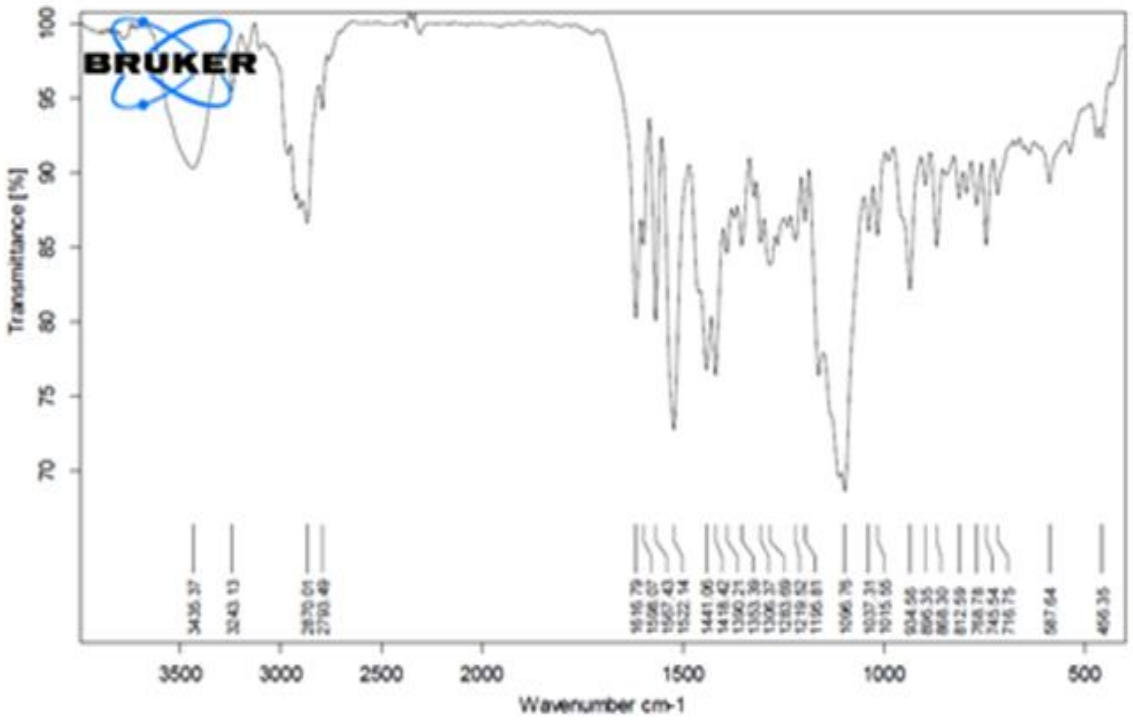
BRUKER
Transmittance [%]
100
95
90
85
80
75
70
3435.37
3243.13
2870.01
2793.49
1616.79
1586.01
1557.43
1522.14
1441.06
1418.42
1380.21
1353.39
1306.37
1283.69
1219.52
1196.81
1096.76
1037.31
1015.58
934.56
895.35
868.30
812.59
768.78
745.54
716.75
587.64
496.35
3500
3000
2500
2000
1500
1000
500
Wavenumber cm-1

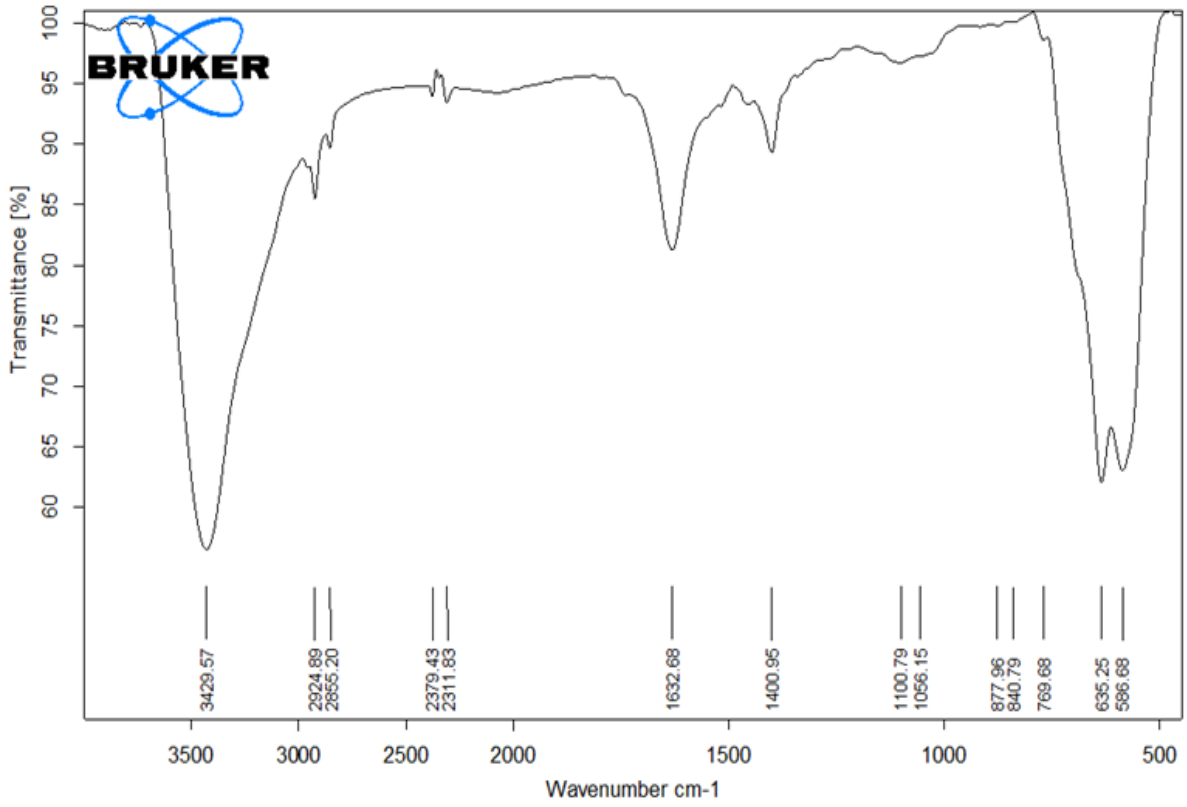
BRUKER
Transmittance [%]
100
95
90
85
80
75
70
65
60
3429.57
2924.89
2855.20
2379.43
2311.83
1632.68
1400.95
1100.79
1056.15
877.96
840.79
769.68
635.25
586.68
3500
3000
2500
2000
1500
1000
500
Wavenumber cm-1

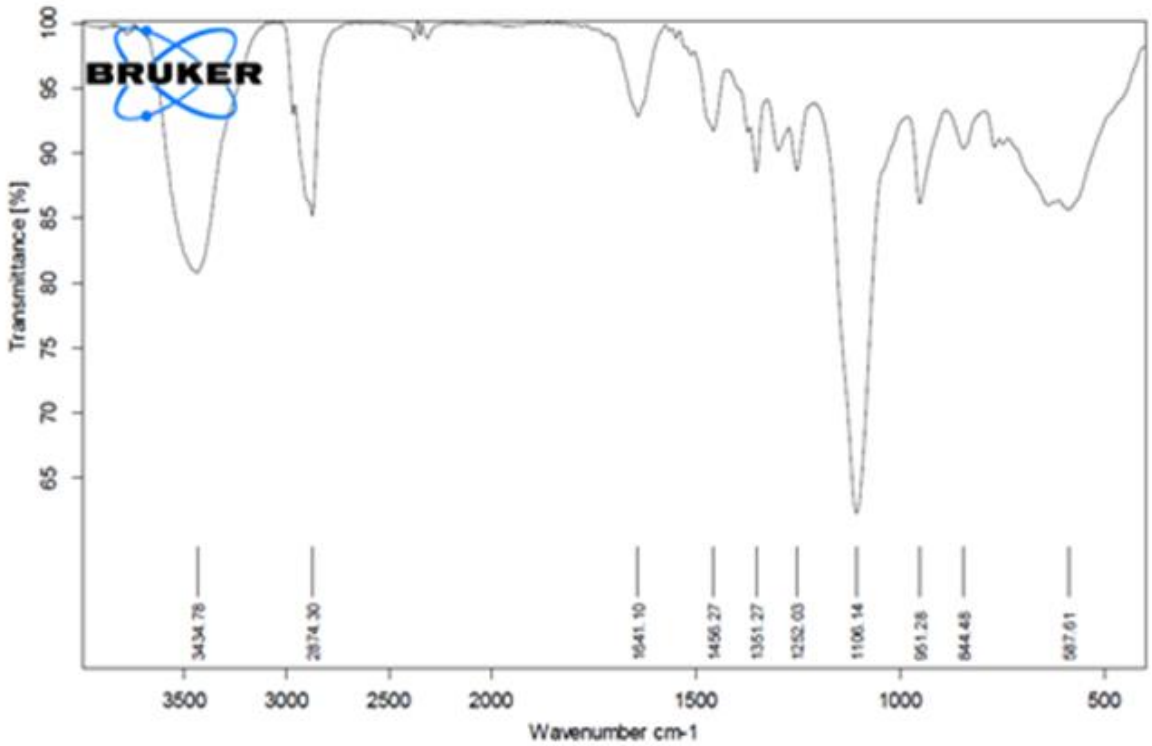
BRUKER
Transmittance [%]
100
95
90
85
80
75
70
65
3434.78
2874.30
1641.10
1456.27
1351.27
1252.03
1106.14
1051.28
844.48
687.61
3500
3000
2500
2000
1500
1000
500
Wavenumber cm-1

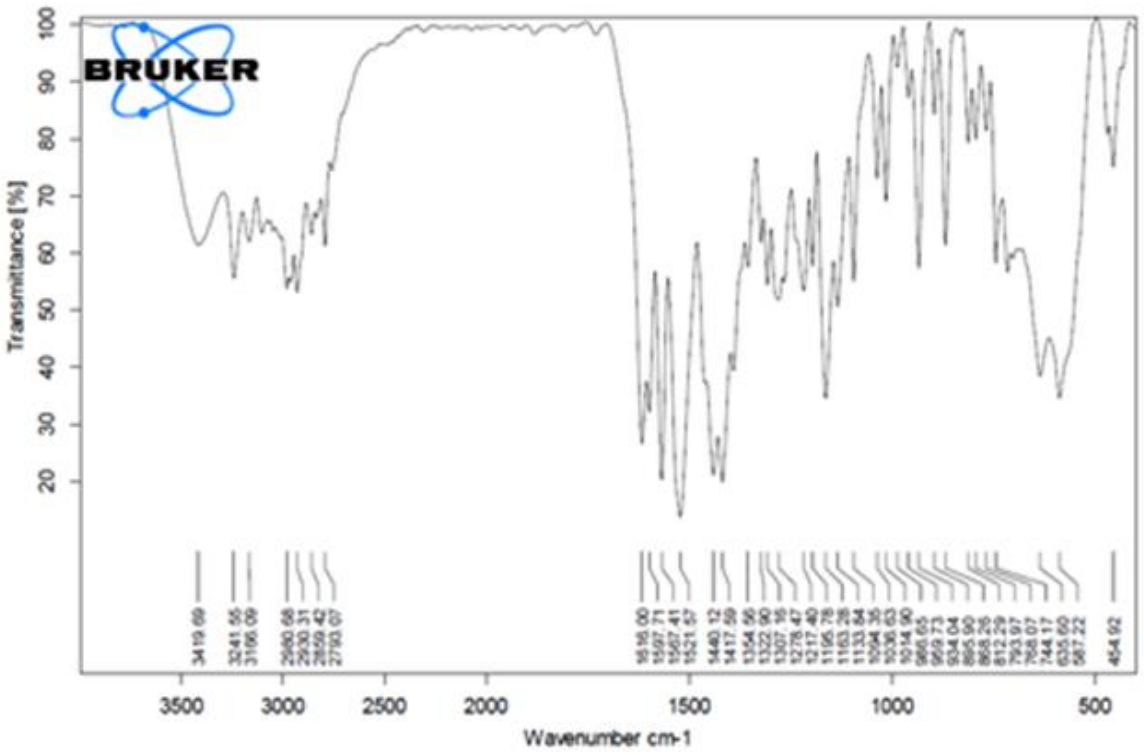

Fig. 4.7. FTIR spectra of Fe_3O_4 NPs Pluronic F-127(surfactant) Brigatinib Fe_3O_4@L-tyrosine and Fe_3O_4@L-tyr/P. Fe_3O_4@L-tyr/P@ Brigatinib. Fe_3O_4@L-Histidine and Fe_3O_4@L-His/P. Fe_3O_4@L-His/P@ Brigatinib. Fe_3O_4@L-Proline and Fe_3O_4@L-Pro/P. Fe_3O_4@L-Pro/P@ Brigatinib.

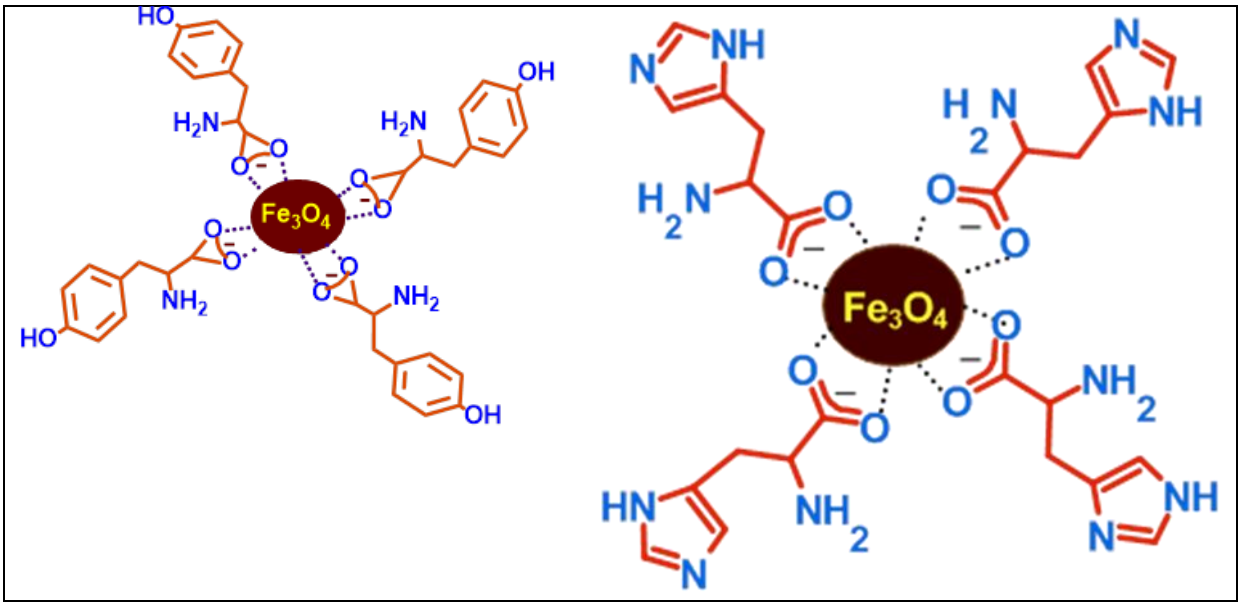

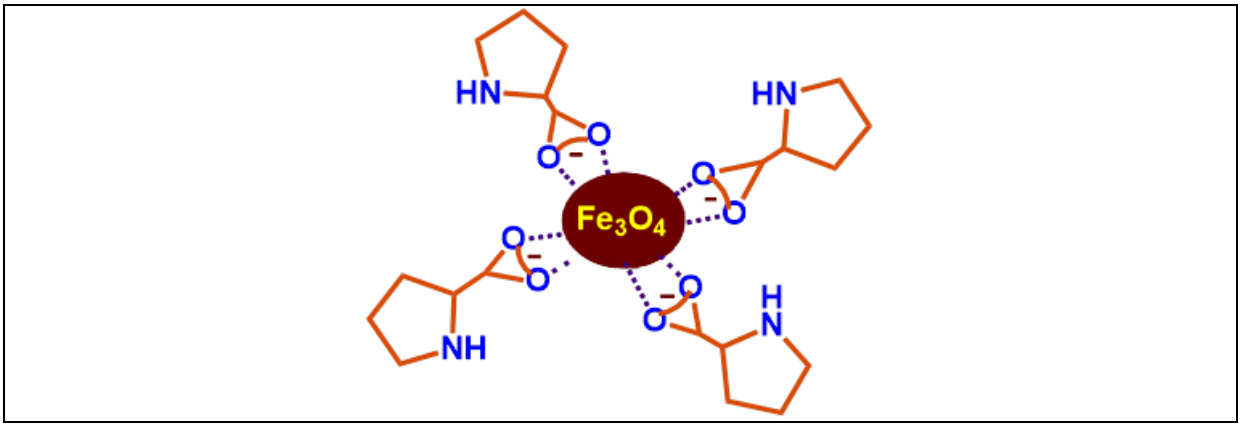

Fig. 4.8. Proposed interaction of L-Tyrosine, L-Proline and L-Histidine molecules with the surface of Fe_3O_4 NPs based on FTIR spectroscopy.

Magnetic properties of the synthesized Fe_3O_4/AA. The shape of magnetization curve (Figure 4.9) indicates superparamagnetic behavior in presence of magnetic field.

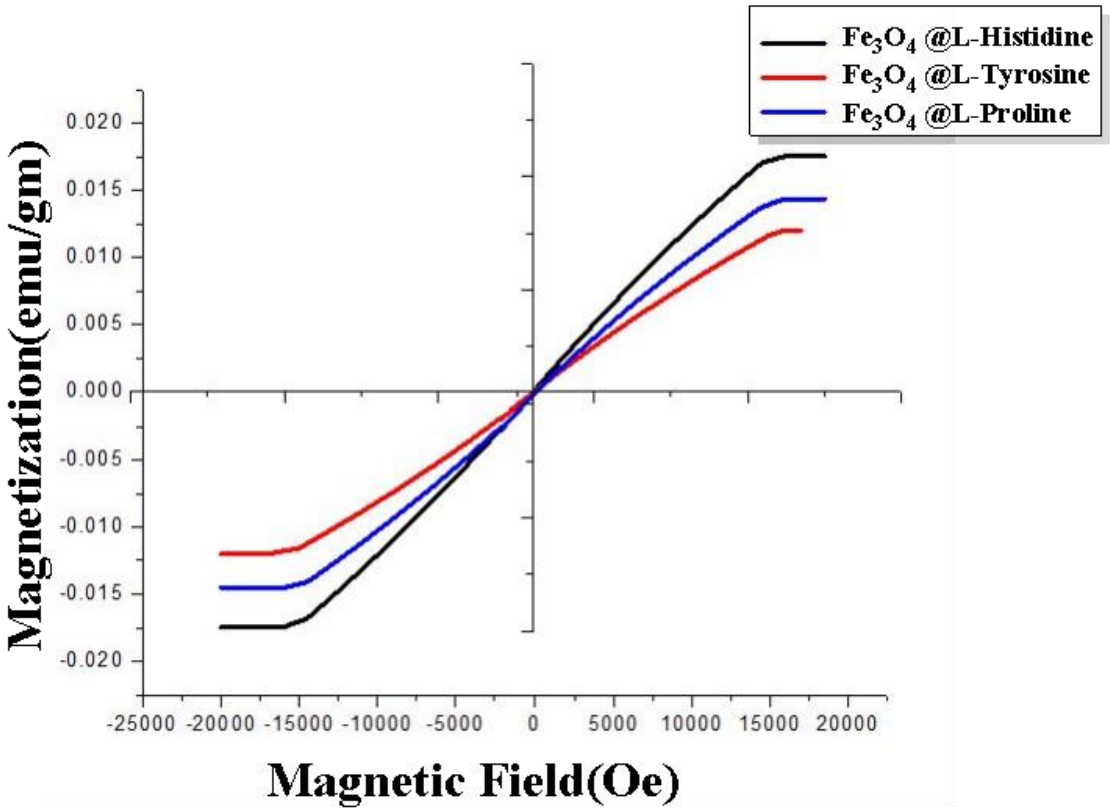

Fig. 4.9. Magnetization curve at room temperature for AA/Fe_3O_4 nanoparticles.

To confirm the stability of the material, a thermal analysis of all the samples was carried out (Figure 4.10). It can be observed from the thermograms that all the samples exhibit two kinds of weight loss in the range of 150 ^{o}C and around 250 °C due to bulk and interior surface-bound water, respectively. The weight loss above 100 °C is continued and persisted till 150 °C, confirming the presence of inner sphere H-bonded water. The weight losses at higher temperatures are due to the carbonization of organic material, confirming the presence of a pluronic layer at the outer shell. Overall, the material is stable up to 450 ^{o}C.

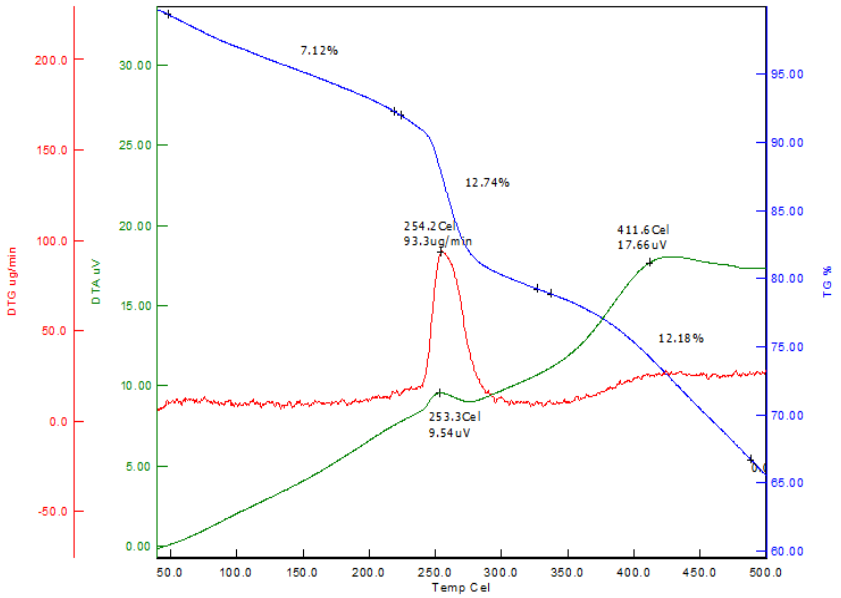

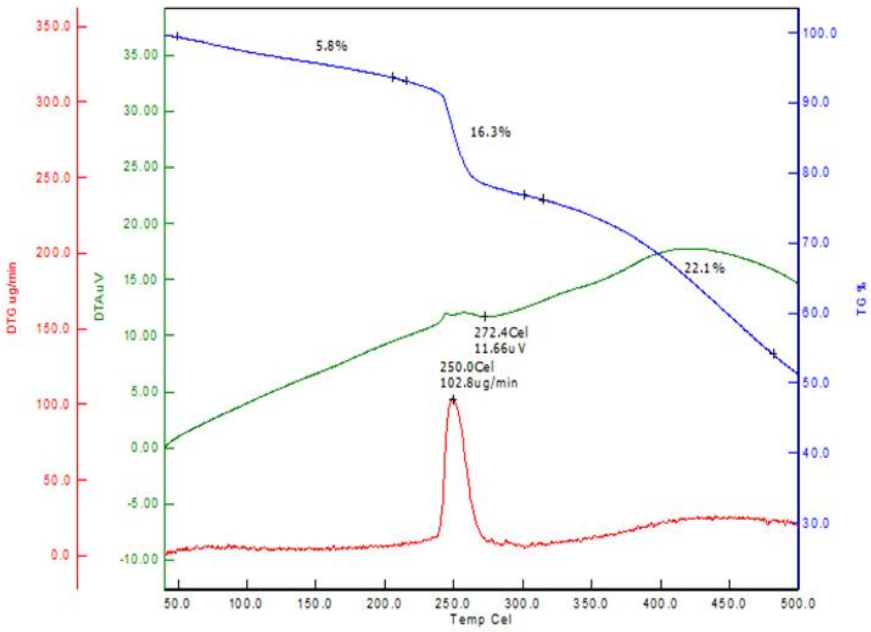

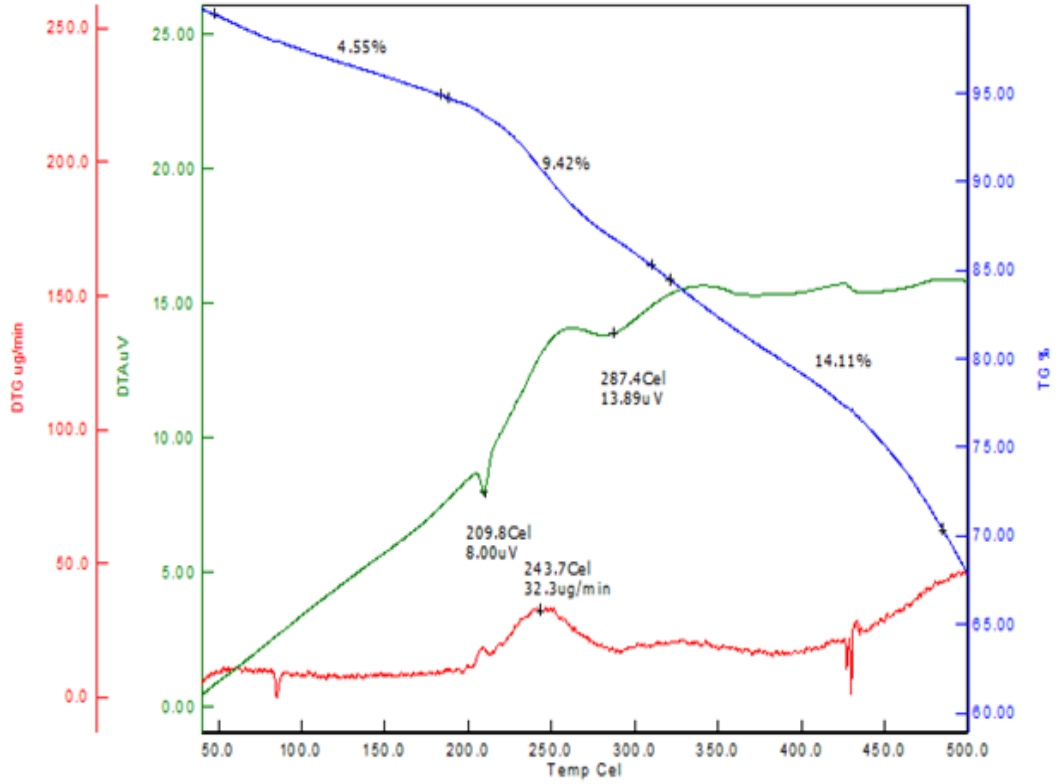

Fig. 4.10. Thermal analysis of as-synthesized Fe_3O_4@L-tyr/P and Fe3O4@L-His/P, Fe_3O_4@L-pro/P.

4.5. *In vitro* drug release kinetics, cell viability and cytotoxicity studies

The kinetics of the *in vitro* release of imatinib from Fe_3O_4/Tyr/P NPs was studied in an aqueous PBS solution at pH 7.4 (Figure 4.11). It can be observed that initially ca. 30% drug was released within the first 5 h and it was stabilized at 48 h with an overall 40.5% release. Interestingly, Fe_3O_4/Hist/P NPs the drug release became 51.23% was released at the end of 100 h. Approximately, 60% of the drug was released at the end of 40 h Fe_3O_4/L-Pro/P NPs. This experiment shows that the developed NPs magnetic micelles have excellent sustained drug release capacity.

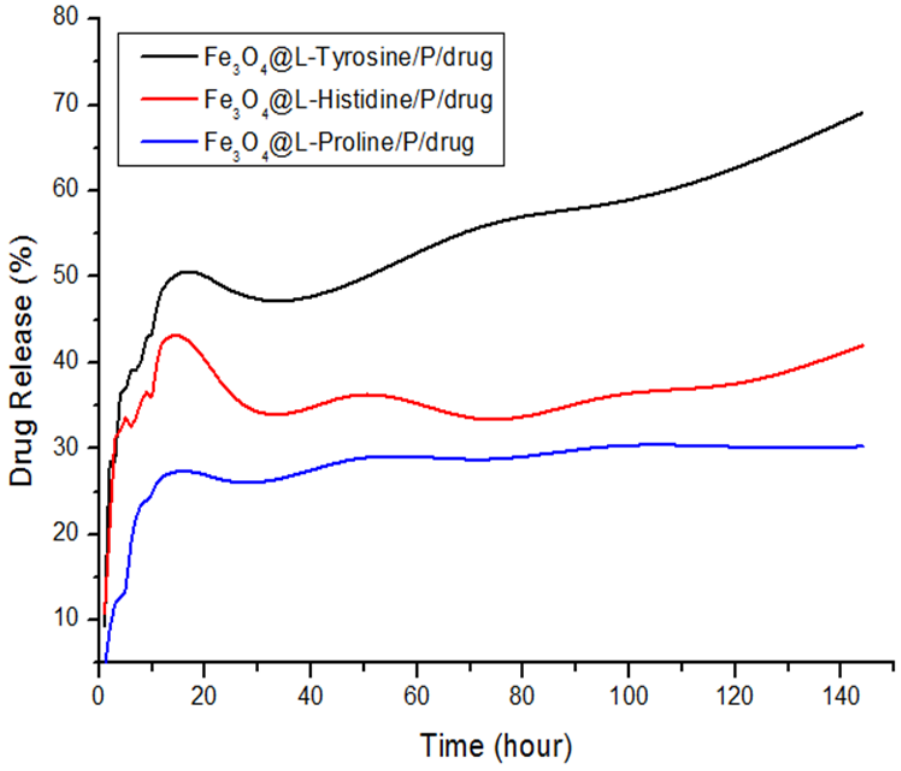

Fig. 4.11. Percentage release of brigatinib from Fe_3O_4@ L-AA/P/bg. The drug released Fe_3O_4@ L-pro/P/bg is the earliest as compared to others. However, at the end of three days (72 h), more drug is released from Fe_3O_4@ L-Tyr/P/bg and Fe_3O_4@ L-His/P/bg than Fe_3O_4@ L-pro/P/bg ones.

4.5.1. *In vitro* drug release kinetics

To study the drug release kinetics, three different experiments were performed. This study was carried out at 37 °C and pH 7.4. In each experiment, 3.0 mg of brigatinib loaded magnetic NPs was added to a flask having 30 mL of Na_2HPO_4–NaH_2PO_4 buffer solution. The flask was then kept in a shaker at 37 °C. The release medium was withdrawn at predetermined time intervals (1, 2, 3, 4, 5, 6, 7, 8, 9, 12, 24, 36, 48, 60, 80, 100, 124, 148, 172, and 196 h). The collected samples were analyzed using a UV–Visible spectrophotometer (Perkin-Elmer Lambda 35) to determine the amount of brigatinib released (λmax 284 nm) Figure 4.12.

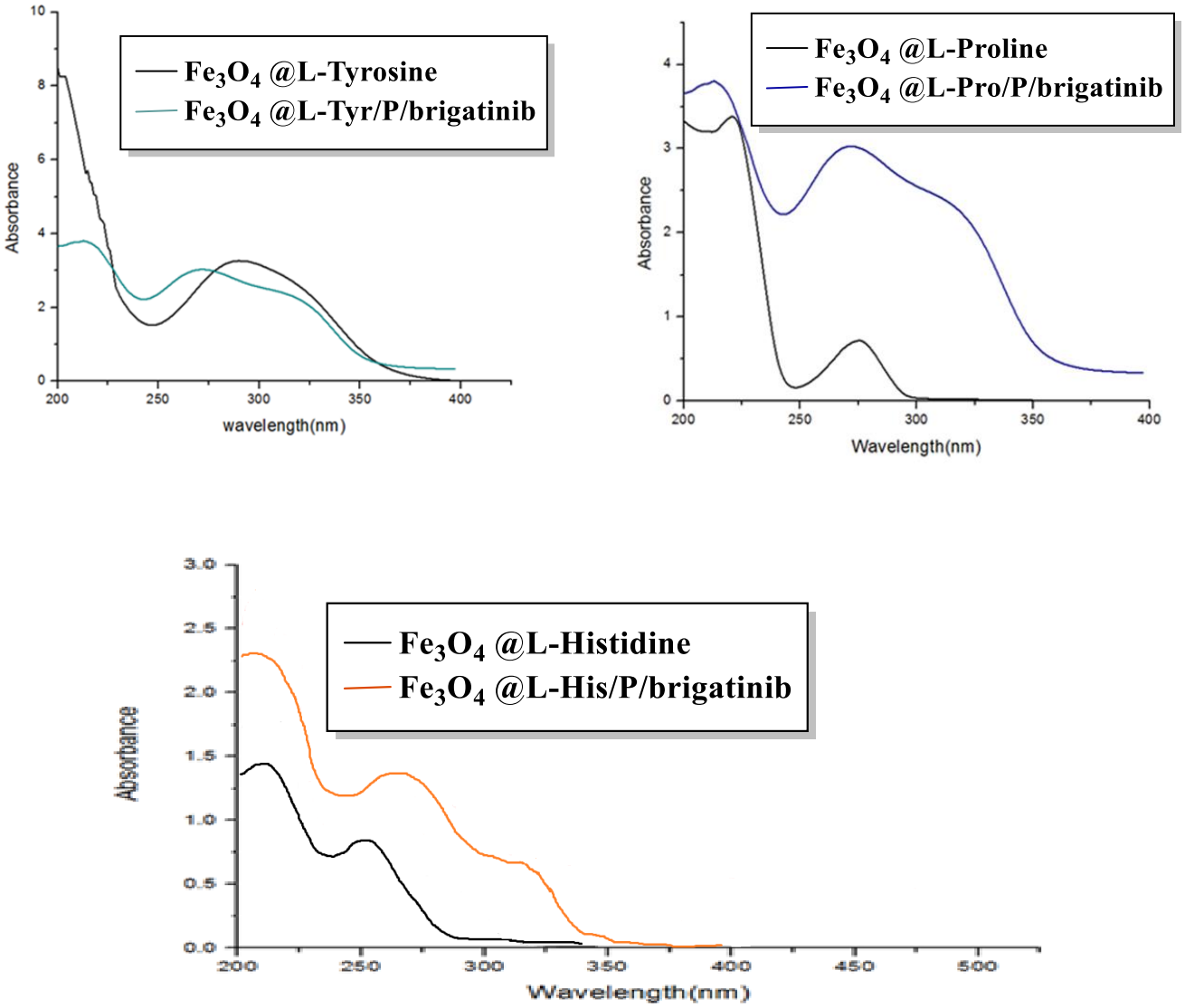

Fig. 4.12. UV-vis studies for control release of brigatinib for as synthesized Fe_3O_4/L-AA/P NPs.

4.5.2. Clonogenic Assay

We used clonogenic assay to determine the colony forming ability of cells under the effect of different treatments. For this assay cells were seeded in 6-well plates at their log phase. A thousand cells per well were plated and incubated in the total media (DMEM low glucose, 10% FBS, 1% antibiotic solution). These were treated with the Fe_3O_4@AA/P/bg and bared brigatinib drugs for 48 hours. Medium was then replaced with new media without any added drugs or formulations. Colonies were stained with crystal violet after 5 days of treatment. The

numbers of colonies containing at least 50 cells were counted using the imageJ software (NIH, USA). The percentage colonies formed were calculated from dividing the number of colonies with a product of number of cells plated and the plating efficiency. Data was obtained in triplicates and graphs were prepared in GraphPad PRISM software (San Diego, CA, USA).

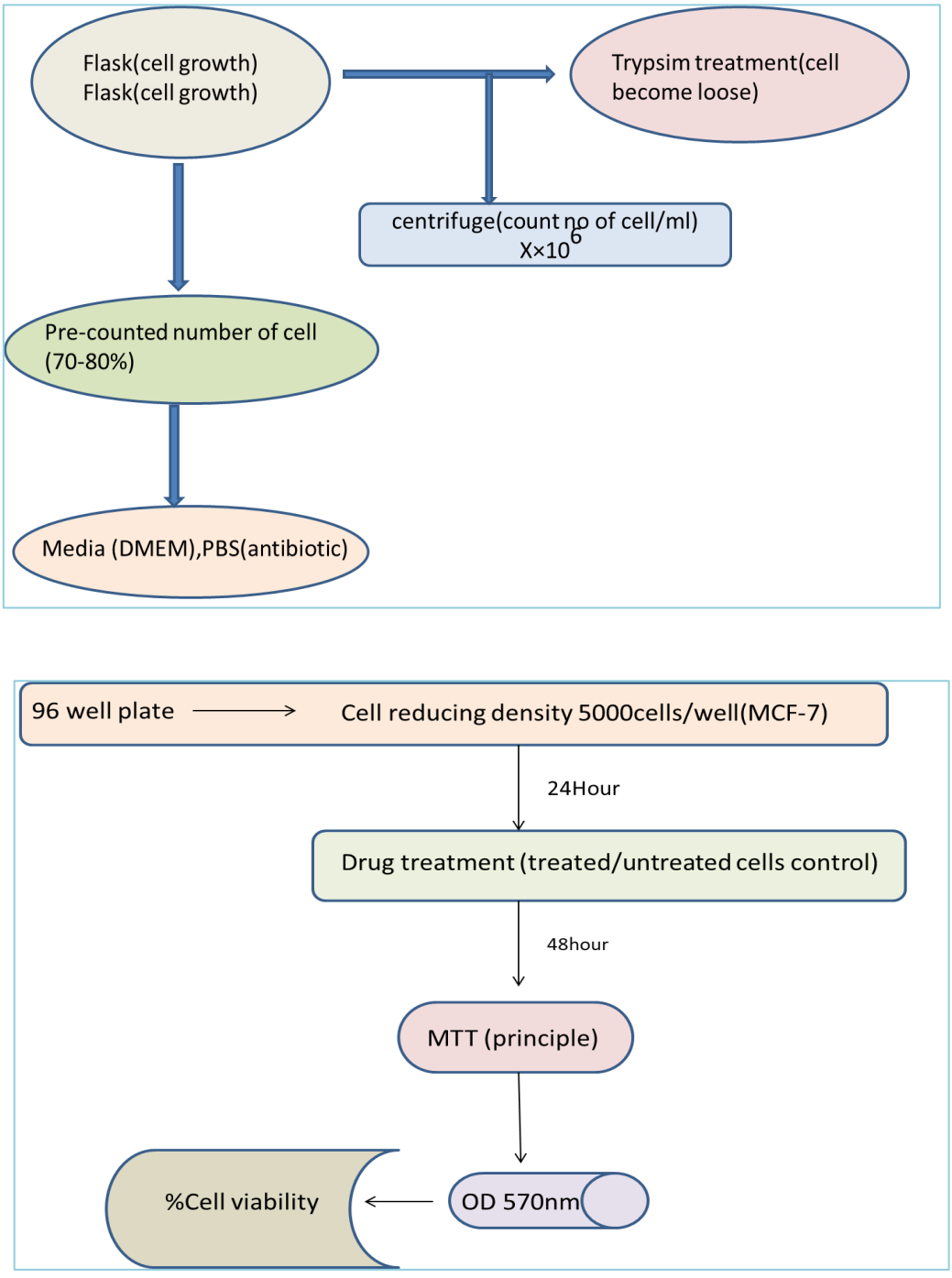

Fig. 4.13. Clonogenic assay

4.5.3. *In Vitro* Cytotoxicity Assay

Trypan blue assay

- Drug was solubilized in DMSO to make a stock concentration of 1mg/mL.
- MCF-7 cells were seeded in 6-well plates at a density of 30,000 cells/well in 0.5 mL medium and left to attach for 24 h at 37 ^{o}C. Subsequently, cells were exposed to drugs in an additional 0.5 mL medium (10, 5, 2.5 and 1.25 µg/mL Brigatinib) for 48 h at 37 ^{o}C.
- Cells were trypsinized and resuspended in equal volumes of medium and Trypan blue (0.05% solution) and counted using a haemocytometer. Trypan blue dye (Invitrogen) exclusion was used to assess cell viability.

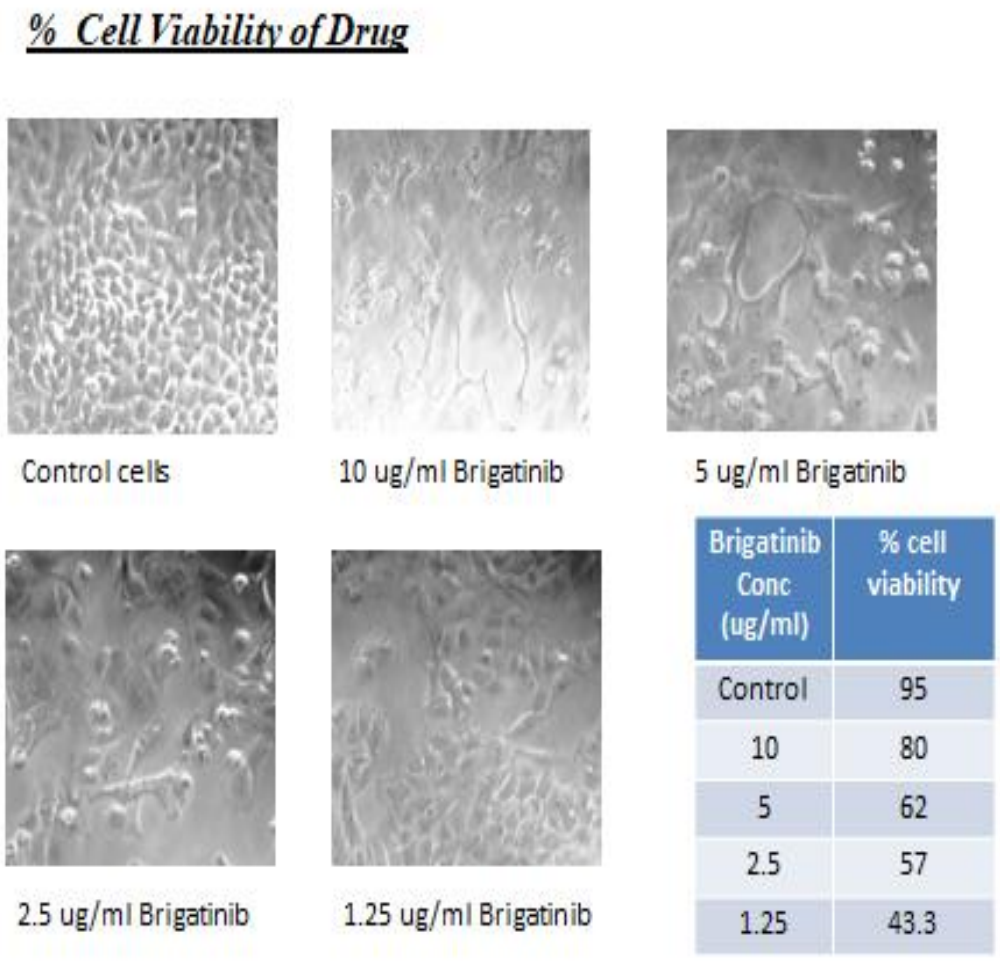

Brigatinib Conc (ug/ml)	% cell viability
Control	95
10	80
5	62
2.5	57
1.25	43.3

Fig. 4.14. Cytotoxicity studies of the drug loaded as-synthesized Fe_3O_4 nanoparticles.

The cytotoxic effect of the synthesized USIONs with or without the drug was studied by MTT assay, on the MCF47 and A549 for human breast cancer and lung cancer cell lines,

respectively (Figure 4.15). The bare drug remains inactive toward cell viability at microgram level dosage. Its 6 µg/mL dosage induce 40% cell death. However, the drug-loaded USIONs (Fe_3O_4@AA/P) affect it at the same level of dosage. In the case of the blank carrier (Fe_3O_4@AA/P), the % cell viability remains basal even at higher dosages emphasizing the safety of the developed delivery platforms. Fe_3O_4@L-Pro/P/bg boosts the significant cell death (15%) at the same dosage levels as compared to the bare drug (6 µg/mL). Fe_3O_4@L-Tyr/P/bg system and Fe_3O_4@L-Hist/P/bg NPs induce the less cell death at the same concentration and does not reduce the cell numbers even if it can release the drug easily (Figure 4.16, 4.17, 4.18 and 4.19).

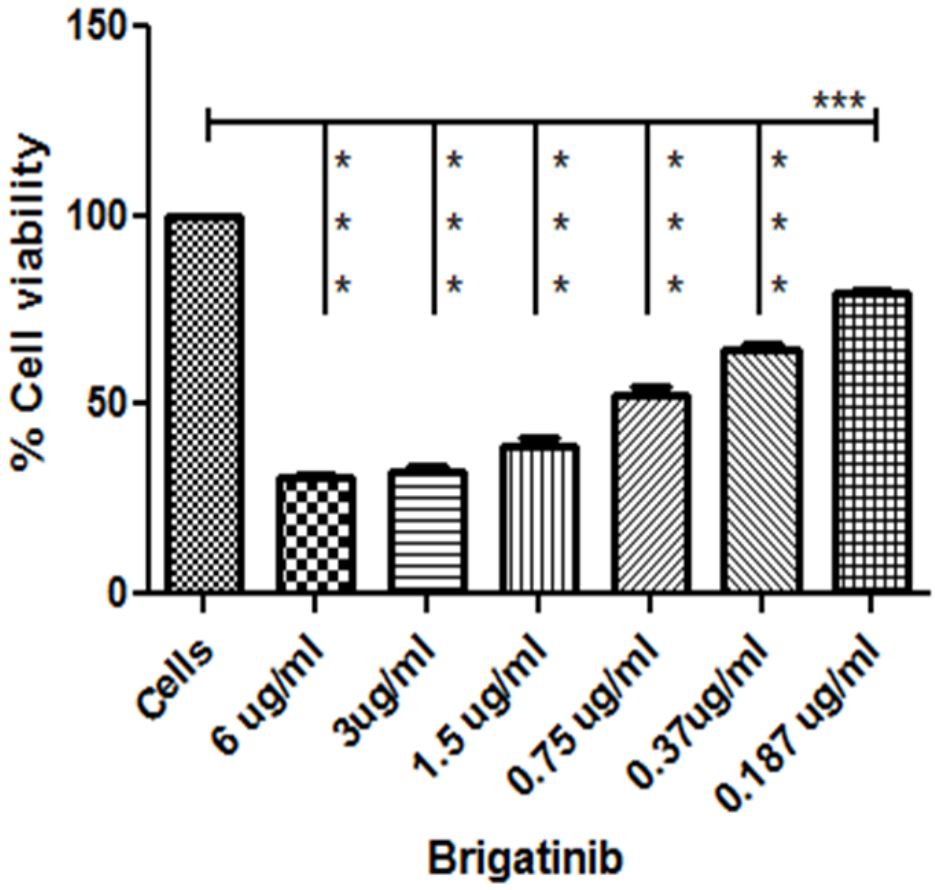

Fig. 4.15. MTT Assay on Drug (brigatinib).

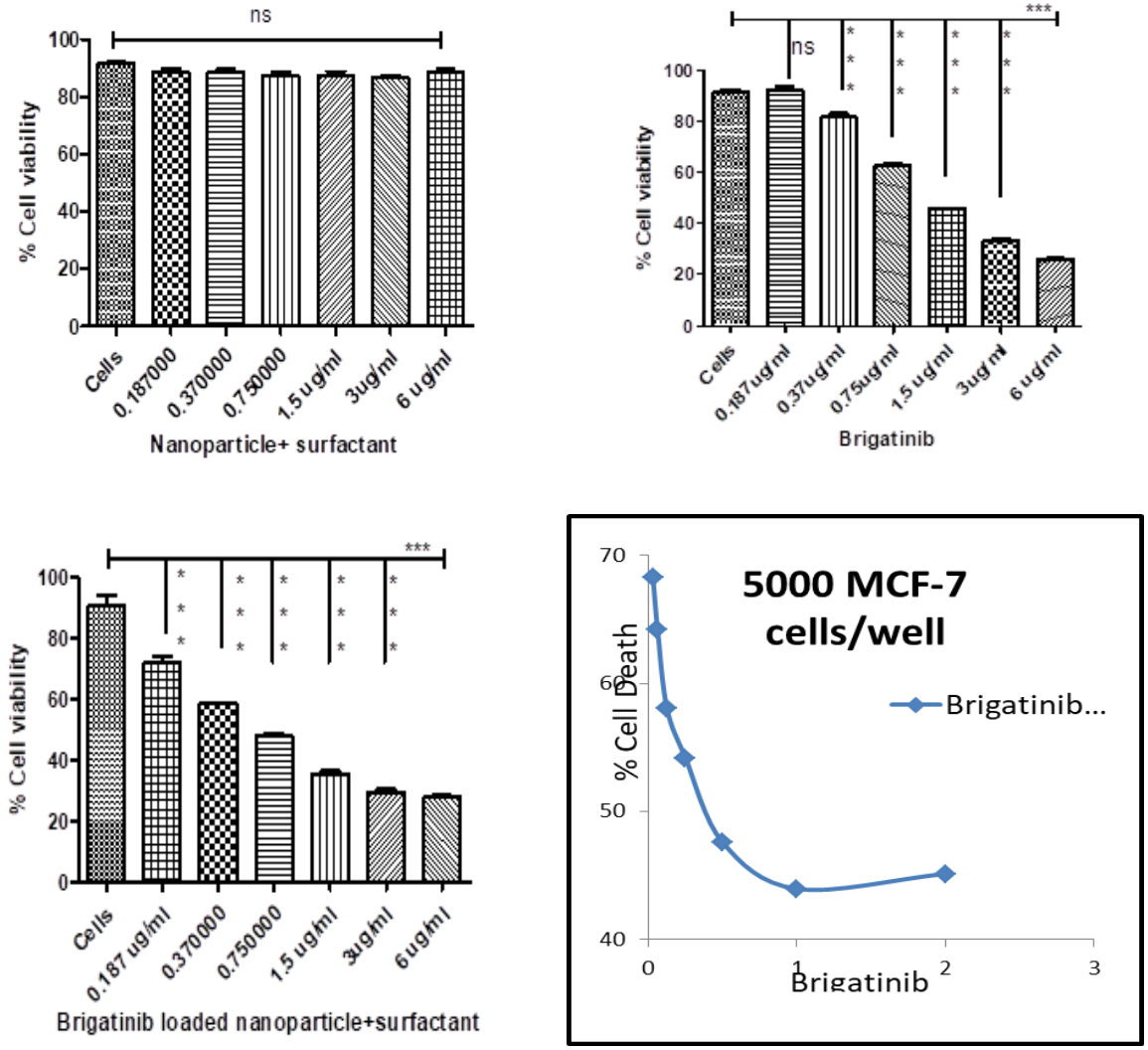

Fig. 4.16. MTT assay of as-synthesized drug loaded Fe_3O_4 nanoparticles on human MCF 7 cell-line.

A. No significant change in cell viability was observed on treatment with nanoparticle coated with surfactant alone (n=3).

B. A significant cell death was observed on treatment with brigatinib alone at a dose greater than 0.187 ug/mL (n=3).

C. A significantly enhanced cell death was observed in brigatinib loaded nanoparticle coated with surfactant (n=3).

(ns= non-significant, ***p<0.001)

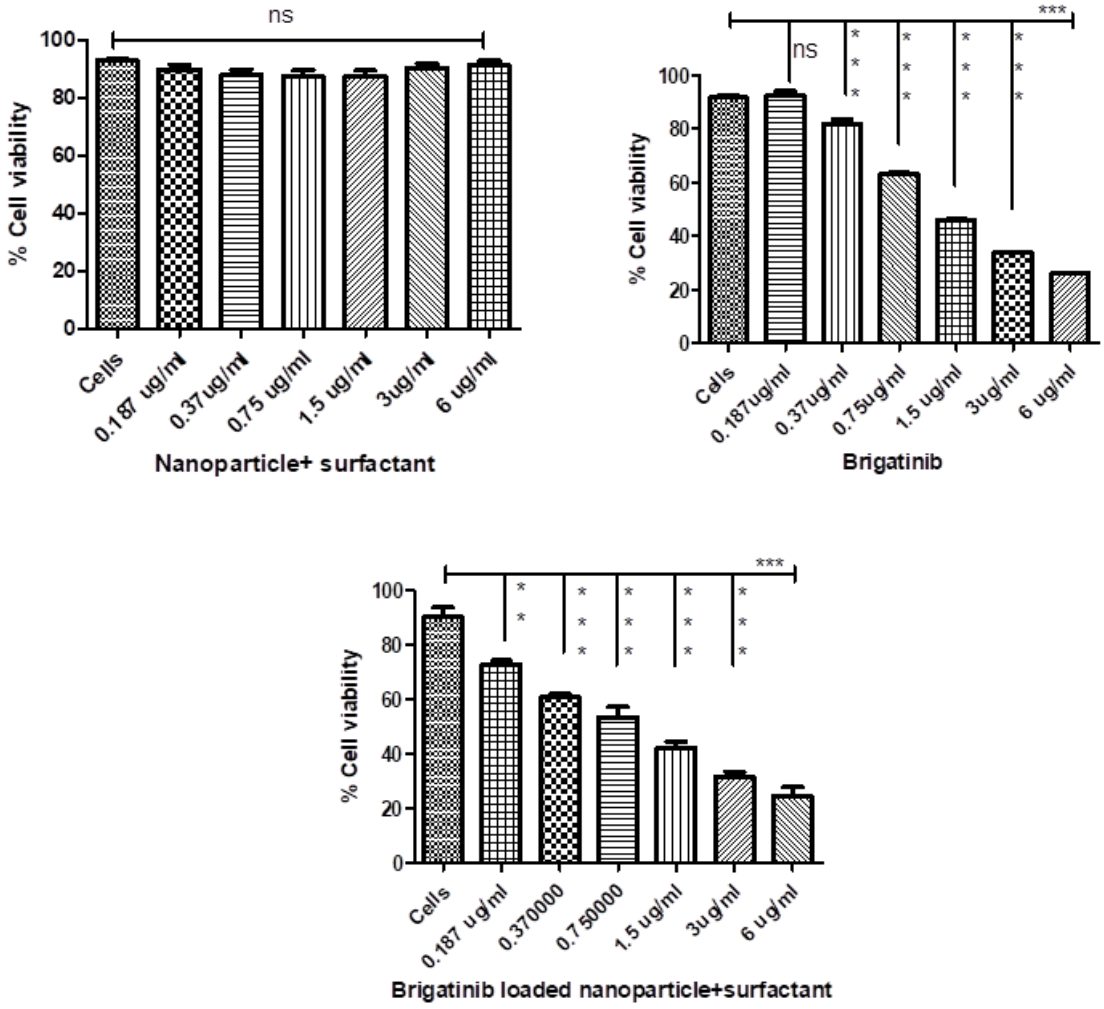

Fig. 4.17. MTT assay A549 L-Tyrosine coated NPs

A. No significant change in cell viability was observed on treatment with nanoparticle coated with surfactant alone (n=3).

B. A significant cell death was observed on treatment with brigatinib alone at a dose greater than 0.187 ug/mL (n=3).

C. A significantly enhanced cell death was observed in brigatinib loaded nanoparticle coated with surfactant (n=3).

(ns= non significant, **p<0.01 and ***p<0.001)

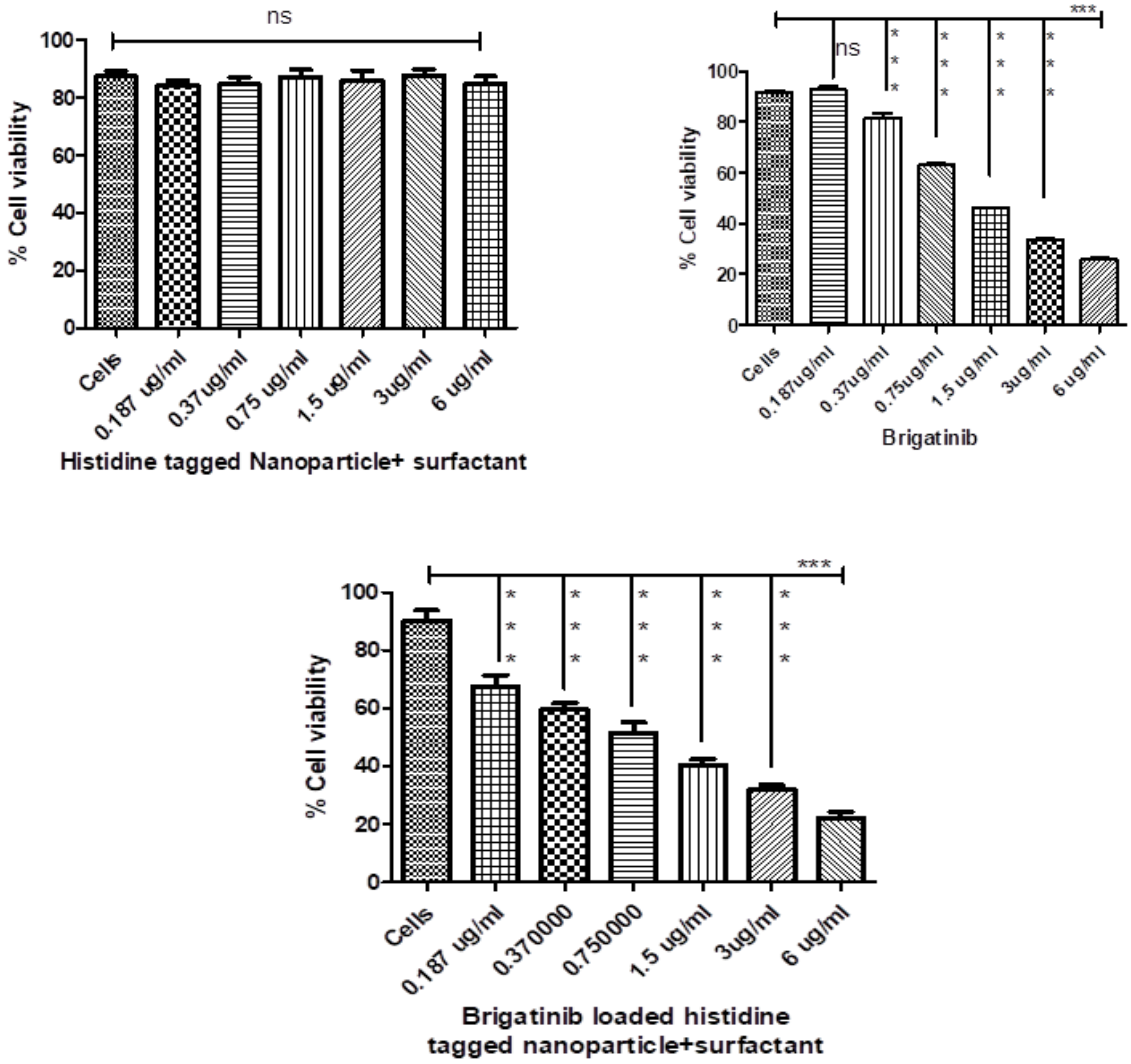

Fig. 4.18. MTT assay A549 L-Histidine Coated NPs.

A. No significant change in cell viability was observed on treatment with histidine tagged nanoparticle coated with surfactant alone (n=3).

B. A significant cell death was observed on treatment with brigatinib alone at a dose greater than 0.187 ug/mL (n=3).

C. A significantly enhanced cell death was observed in brigatinib loaded histidine tagged nanoparticle coated with surfactant (n=3). (ns= non-significant,***p<0.001)

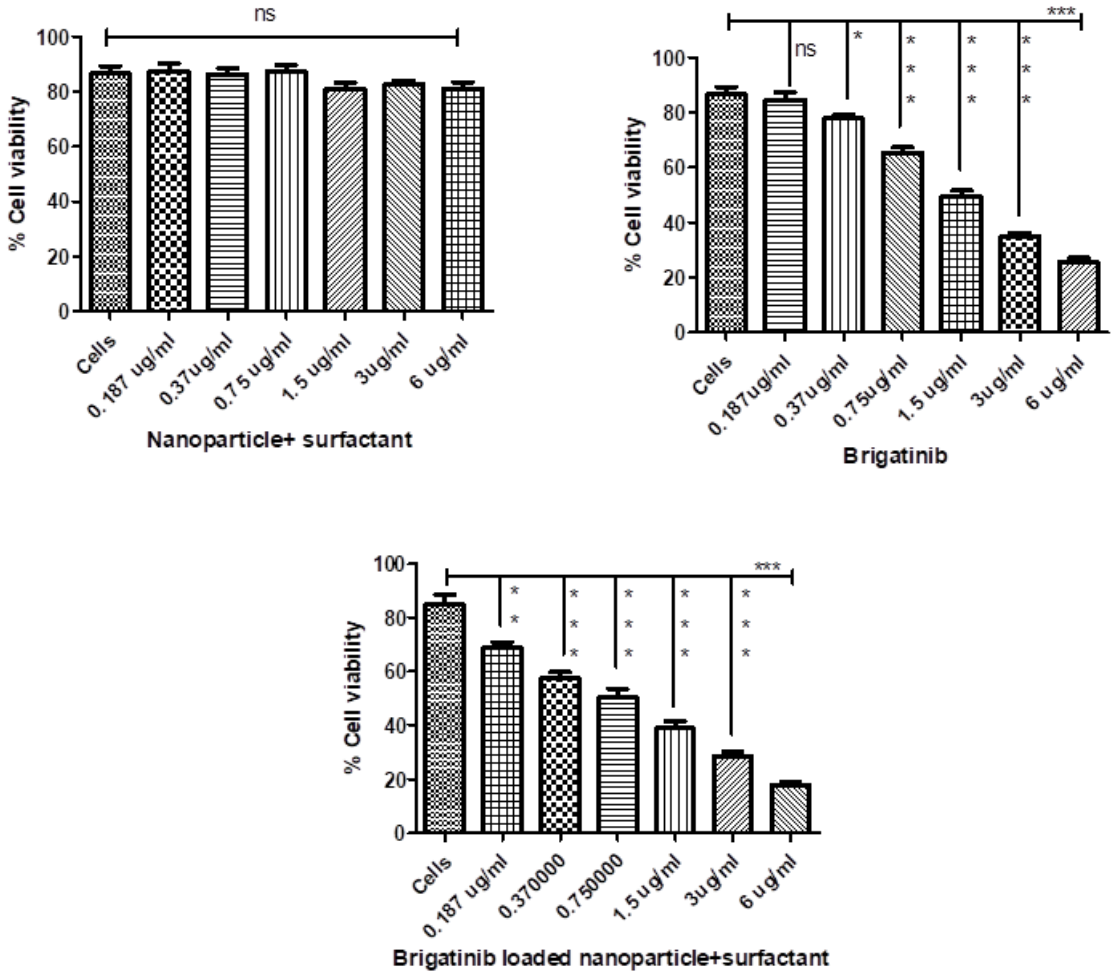

Fig. 4.19. MTT assay A549 L-Proline coated NPs.

A. No significant change in cell viability was observed on treatment with histidine tagged nanoparticle coated with surfactant alone (n=3).

B. A significant cell death was observed on treatment with brigatinib alone at a dose greater than 0.187 ug/mL (n=3).

C. A significantly enhanced cell death was observed in brigatinib loaded proline tagged nanoparticle coated with surfactant (n=3). (ns= non-significant, ***p<0.001)

A significantly enhanced cell death was observed in Brigatinib loaded proline tagged nanoparticle coated with surfactant even at 0.187ug/mL (n=3). (***p<0.001)

Proline tagging has increased the efficacy of Brigatinib.

In other words, Brigatinib loaded nanoparticles cause significant cell death even at a concentration as low as 0.187ug/mL.

4.6. Conclusion

Synthesis and characterization of different types of (magnetic) nanoparticle systems: To achieve this objective, Fe_3O_4 nanoparticles being capped with various amino acid molecules had been synthesized by simple wet chemical methods.

To design new ligands act as anticancer agents and their anchoring on the surface of the NPs system for sustainable release of the drug at the target site was also the aim of the proposed work. The resulting products were first characterized and their biological activity as an anticancer agent and also their toxicity were evaluated. The results were encouraging. Based on these data, the alteration and modification in the molecular framework of the as-synthesized derivatives were carried out and the effective ligands were anchored on the surface of NPs vehicle. Pluronic-encapsulated and L-Proline-capped Fe_3O_4 magnetic micelles can act as drug delivery platforms to load the hydrophobic anti-cancer drug brigatinib in their hydrophobic shells.

From this study, it can be concluded that: (i) drug can makes stable bonding with nanoparticles on its surface by intermolecular H-bonding or by entrapping inside cavities; (ii) pluronic like copolymeric surfactant which are capable to acquire ‘mild’ positive charge in the intra cellular environment can provide stealth and flexible surface to the delivery vehicle. More experiments are needed to establish this claim for eukaryotic cells in a large scale. Hence, iron oxide nanoparticles can serve as non-toxic, biodegradable and safe vectors to load a variety of drug/gene of useful products like enzymes, proteins, peptides, hormones etc into the cells. Such a carrier can also be used for delivering genes into eukaryotic cells and can be a potential candidate for use in gene therapy also.

4.7. References

1. A. Jemal, F. Bray, M. M. Center, J. Ferlay, E. Ward and D. Forman, Ca-Cancer, J. Clin., 61, 69, (2011).
2. R. Siegel, D. Naishadham and A. Jemal, Ca-Cancer J. Clin., 63, 11, (2013).
3. N. Milosavljevic, C. Duranton, N. Djerbi, P. H. Puech, P. Gounon, D. Lagadic-Gossmann, M. T. Dimanche-Boitrel, C. Rauch, M. Tauc, L. Counillon and M. Poe¨t, Cancer Res., 70, 7514, (2010).
4. M. C. Perry, The Chemotherapy Source Book, Lippincott Williams and Wilkins, 5th edn, (2012).
5. G. Tiwari, R. Tiwari and A. K. Rai, J. Pharm. BioAllied Sci., 2, 72, (2010).
6. J. Zhang and P. X. Ma, Adv. Drug Delivery Rev., 65, 1215, (2013).
7. U. Kedar, P. Phutane, S. Shidhaye and V. Kadam, Nanomedicine, 6, 714, (2010).
8. G. S. Kwona and T. Okano, Adv. Drug Delivery Rev., 21, 107, (1996).
9. A. M.Mintzer and E. E. Simanek, Chem. Rev., 109, 259, (2009).
10. P. Tanner, P. Baumann, R. Enea, O. Onaca, C. Palivan and W. Meier, Acc. Chem. Res., 44, 1039, (2011).
11. Q. Jin, Y. Deng, X. Chen, J. Ji, ACS Nano, 13, 954, (2019).
12. H. Hatakeyama, H. Akita, H. Harashima, Biol. Pharm. Bull. 36, 892, (2013).
13. H. Hatakeyama, H. Akita, H. Harashima, Adv. Drug Delivery Rev., 63, 152, (2011).
14. A. V. Kabanov, E. V. Batrakova, V. Y. Alakhov, J. Control. Release, 82, 189, (2002).
15. A. V. Kabanov, P. Lemieux, S. Vinogradov, V. Alakhov, Adv. Drug Deliv. Rev., 54, 223, (2002).
16. M.-M. Fan, X. Zhang, J. Qin, B. -J. Li, X. Sun, S. Zhang, Macromol. Rapid Commun., 32, 1533, (2011).
17. M. Kanamala, W. R. Wilson, M. Yang, B. D. Palmer, Z. Wu, Biomaterials, 85, 152, (2016).
18. M. J. Rosen, X. Y. Hua, J. Colloid Interface Sci. 86, 164, (1982).
19. T. Yoshida, T. Kumagai, R. Toyozawa, Cancer Science,114,9(2023).
20. R. Ali, J. Arshad, S. Palacio, R. Mudad ,Dug Des Devel Ther, 569, 13(2019).
21. W.S. Huang, S. Liu, D. Zou, J. Med Chem, 59, 10(2016).
22. S. Popat, O.T. Brustugun , J. Cadranel, Lung Cancer , 157,9(2021).
23. N. Gupta, X. Wang, Clinical Pharmacokinetics, 235,60(2021).
24. D.R. Camidge,H.R. Kim, M.J. Ahn, J Clin Oncol. , 38,31 (2020).

25. K. Ando, K. Akimoto, H. Sato, Cancers,12 ,4 (2020).
26. I. C. Macdougall, Kidney Int. Suppl., 69, S61, (1999).